iScience

CellPress
OPEN ACCESS

Article

Deleting autotaxin in LysM+ myeloid cells impairs innate tumor immunity in models of metastatic melanoma

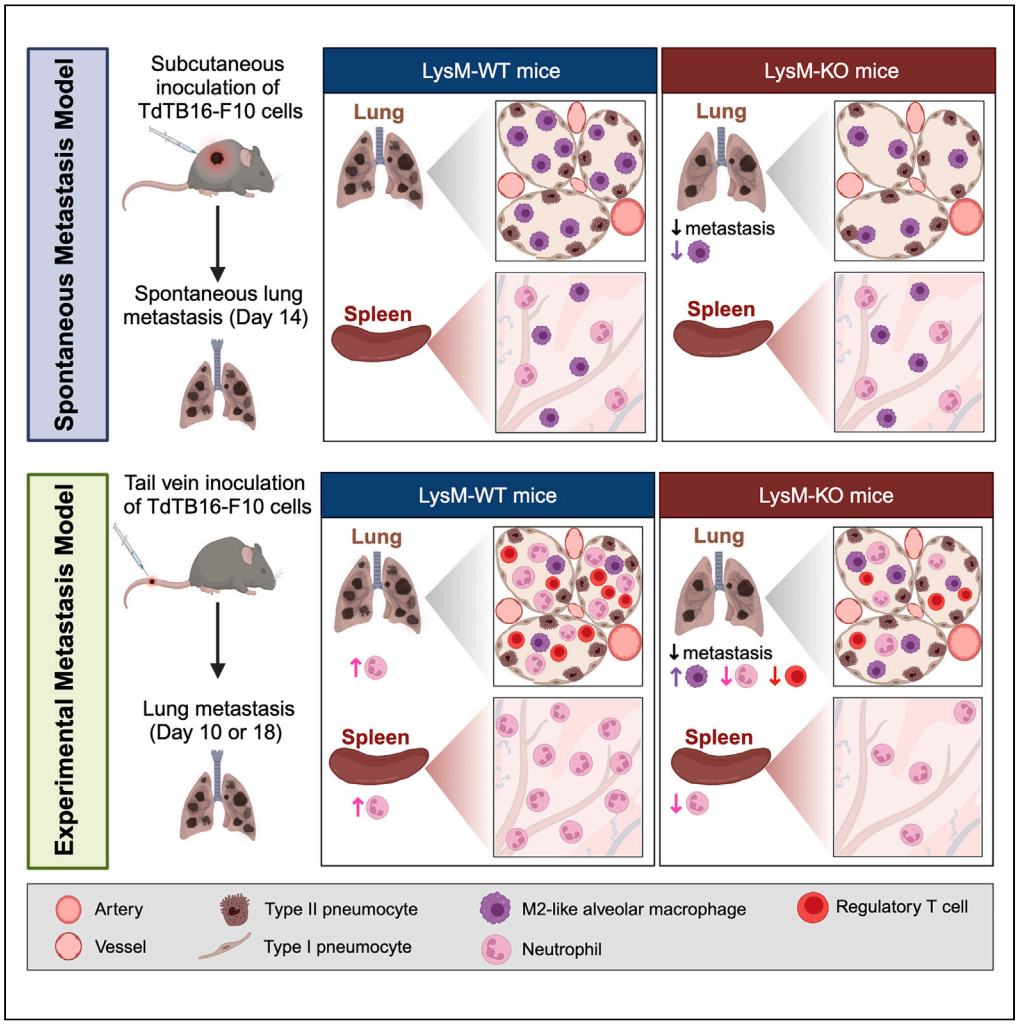

Mélanie A. Dacheux, Derek D. Norman, Yoojin Shin, Gábor J. Tigyi, Sue Chin Lee

gtigyi@uthsc.edu (G.J.T.)
slee84@uthsc.edu (S.C.L.)

Highlights

ATX is expressed by myeloid cells in human primary and metastatic melanomas

Deleting ATX in LysM+ myeloid cells had no effect on primary tumor growth in mice

Deleting ATX in LysM+ myeloid cells reduced melanoma lung metastases in mice

Spontaneous and experimental metastasis models produce distinct immune cell profiles

Dacheux et al., iScience 27, 110971
October 18, 2024
https://doi.org/10.1016/j.isci.2024.110971

iScience

CellPress
OPEN ACCESS

Article

Deleting autotaxin in LysM+ myeloid cells impairs innate tumor immunity in models of metastatic melanoma

Mélanie A. Dacheux,[1] Derek D. Norman,[1] Yoojin Shin,[1] Gábor J. Tigyi,[1,2,3,*] and Sue Chin Lee[1,2,3,4,*]

SUMMARY

Autotaxin (ATX) is a lysophospholipase D that generates lysophosphatidic acid (LPA) and regulates cancer metastasis, therapeutic resistance, and tumor immunity. We found that myeloid cells in human melanoma biopsies abundantly express ATX and investigated its role in modulating innate tumor immunity using two models of melanoma metastasis—spontaneous and experimental. Targeted knockout of ATX in LysM+ myeloid cells in mice (LysM-KO) reduced both spontaneous and experimental B16-F10 melanoma metastases by ≥ 50%. Immunoprofiling revealed differences in M2-like alveolar macrophages, neutrophils and regulatory T cells in the metastatic lungs of LysM-WT versus LysM-KO that are model-dependent. These differences extend systemically, with LysM-KO mice bearing experimental metastasis having fewer neutrophils in the spleen than LysM-WT mice. Our results show that (1) LysM+ myeloid cells are an important source of ATX/LPA that promote melanoma metastasis by altering innate tumor immunity, and (2) intratumor and systemic immune profiles vary dynamically during disease progression and are model-dependent.

INTRODUCTION

Autotaxin (ATX), encoded by the human ectonucleotide pyrophosphatase phosphodiesterase 2 (*ENPP2*) gene, is a lysophospholipase D enzyme responsible for the generation of lysophosphatidic acid (LPA) from lysophospholipids. LPA is a growth factor-like lipid mediator that activates six different G protein-coupled LPA receptors (LPAR 1–6) as well as the intracellular peroxisome proliferator-activated receptor gamma (PPARγ). ATX is produced and secreted not only by cancer and cancer stem-like cells, but also by stromal and immune cells that are present in the tumor microenvironment (TME).[1–3] The ATX-LPA-LPAR signaling axis is upregulated in many aggressive forms of cancer, where it is associated with metastatic progression, therapeutic resistance, and poor prognosis.[4,5]

There is growing evidence that ATX and LPA play a profound role in modulating tumor immunity. Patients with stage IV melanoma who are refractory to immunotherapy were found to have higher levels of LPA.[6] Likewise, the levels of ATX and LPA were elevated in a mouse model of non-small cell lung cancer that developed resistance to anti-PD-L1 immunotherapy. By combining an ATX inhibitor with anti-PD-1 immunotherapy, the anti-tumor immune response in these mice was restored.[7] Bioinformatic analysis revealed that ATX expression in human melanoma tumors is linked to an exhausted cytotoxic T lymphocyte (CTL) signature.[6] Furthermore, high levels of ATX and LPA in the TME suppress the infiltration of CTLs into the tumor regions.[7,8] Both naive $CD8^+$ T lymphocytes and CTLs express LPAR5 and LPAR6. LPAR5 impairs CTL killing function by blocking the formation of the immunological synapse, whereas LPAR6 inhibits the motility and migration of CTLs *in vitro*.[8–11] Altogether, these studies suggest that the ATX-LPAR signaling axis impedes adaptive tumor immunity.

One of the most common causes of immunotherapy failure is the establishment of an immunosuppressive TME. This is driven in part by cells of the myeloid lineage that acquire a tumor-promoting phenotype.[12,13] Myeloid cell populations in the TME that help tumor cells evade immune surveillance and contribute to cancer progression and metastasis include tumor-associated neutrophils (TANs), tumor-associated macrophages (TAMs), dendritic cells (DCs), eosinophils, and myeloid-derived suppressor cells (MDSCs).[13] However, there has been little investigation of the role of ATX in modulating innate immune responses against cancer. One study reported that TAMs in the ascites of ovarian cancer have high ATX expression,[14] whereas another showed that deletion of ATX in macrophages diminishes the formation of early lung neoplastic lesions.[15] More recently, ATX has been shown to suppress eosinophil infiltration into tumor regions in a mouse model of pancreatic cancer.[16]

In the present study, we provide evidence that ATX is abundantly expressed in both human and mouse myeloid cells. Deleting ATX in LysM+ myeloid lineage cells (LysM-KO mice) substantially reduced the metastatic burden of B16-F10 melanomas by ≥ 50% compared to

[1]Department of Physiology, University of Tennessee Health Science Center Memphis, 3N. Dunlap Street, Memphis, TN 38163, USA
[2]These authors contributed equally
[3]Senior author
[4]Lead contact
*Correspondence: gtigyi@uthsc.edu (G.J.T.), slee84@uthsc.edu (S.C.L.)
https://doi.org/10.1016/j.isci.2024.110971

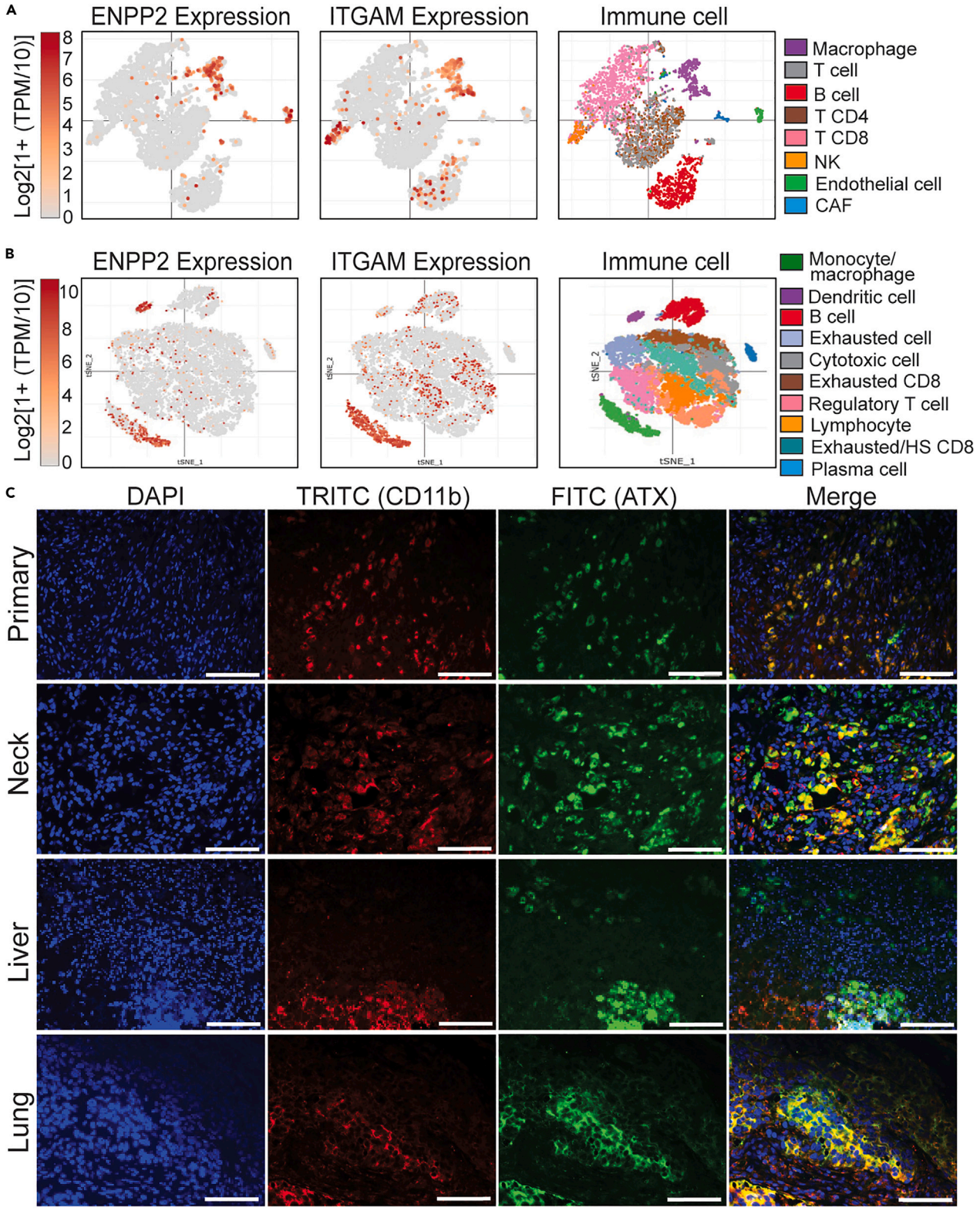
A
ENPP2 Expression
ITGAM Expression
Immune cell
Log2[1+ (TPM/10)]
8
7
6
5
4
3
2
1
0
Macrophage
T cell
B cell
T CD4
T CD8
NK
Endothelial cell
CAF
B
ENPP2 Expression
ITGAM Expression
Immune cell
Log2[1+ (TPM/10)]
10
8
6
4
2
0
tSNE_1
tSNE_2
Monocyte/ macrophage
Dendritic cell
B cell
Exhausted cell
Cytotoxic cell
Exhausted CD8
Regulatory T cell
Lymphocyte
Exhausted/HS CD8
Plasma cell
C
DAPI
TRITC (CD11b)
FITC (ATX)
Merge
Primary
Neck
Liver
Lung

Figure 1. Expression of ATX in CD11b^{+} myeloid cells in primary and metastatic human melanomas

T-distributed stochastic neighbor embedding (t-SNE) plots of ENPP2 (ATX) and ITGAM (CD11b) expression, and corresponding immune cell populations in (A) human melanoma tumors and (B) melanoma tumors treated with checkpoint inhibitors. T-SNE plots were generated using the Single Cell Portal (https://singlecell.broadinstitute.org/single_cell). NK, natural killer cells; CAF, cancer associated fibroblasts.

(C) Representative immunofluorescence staining of ATX and CD11b in human primary (TriMetis #111889 634A1; #111699 594A1) and metastatic (TriMetis #109960 335B2; #111850 618A3) melanoma sections. Nuclei were counterstained for DAPI (blue), and cells were stained for CD11b (red; TRITC channel) and ATX (green; FITC channel). Merged images of all three stains are shown in the fourth panel (left). White scale bars represent 1000 μm.

LysM-WT mice in two models of metastasis—spontaneous metastasis model (SMM) and experimental metastasis model (EMM). We found that LysM-KO mice bearing spontaneous metastasis had fewer M2-like alveolar macrophages than LysM-WT mice. Next, we evaluated differences in immune cell profiles in EMM at two time points: day 10 (D10) and D18, which reflects mid- and late-stage metastasis, respectively. At D10 of EMM, LysM-KO mice had more M2-like alveolar macrophages, but fewer neutrophils and regulatory T cells (Tregs) than LysM-WT mice. The decrease in neutrophil numbers in the lungs of LysM-KO mice persisted to D18 (EMM). Interestingly, we found that metastasis-associated macrophages (MAMs), identified by the markers[17] F4/80^{+}Ly6G^{-}CD11b^{+++}Ly6C$^{-/lo}$, were only present in the lungs of mice bearing experimental metastases at D18. LysM-WT mice were found to have higher number of MAMs in the lungs compared to LysM-KO mice. Differences in myeloid cell populations were also noted systemically, with LysM-KO mice having fewer neutrophils in the spleen than LysM-WT mice. These observations suggest that ATX derived from both macrophages and neutrophils may play differential roles in the metastatic cascade. In both SMM and EMM, LysM-KO mice had decreased levels of 18:2- and 20:4-LPA when compared to LysM-WT mice, indicating that LysM+ myeloid cells could be a potential source for these LPA species. Altogether, our findings identify LysM+ myeloid cells as a source of ATX and LPA that promotes the development of melanoma metastasis by impairing innate tumor immunity.

RESULTS

ATX is expressed in myeloid lineage cells present in primary and metastatic human melanoma biopsies

We first investigated if ATX is expressed in myeloid cells infiltrating human melanoma tumors by analyzing two independent single-cell RNA-seq datasets (scRNA-seq) from the Single Cell Portal database (RRID:SCR_014816).[18,19] The first scRNA-seq dataset was chosen because it has been previously reported that high intratumoral ATX expression (by melanoma tumors and cells of the TME) correlated with reduced CD8 T cell infiltration. Using CD11b/ITGAM as a pan myeloid marker, we found that ATX is abundantly expressed in myeloid cells infiltrating human melanoma tumors (Figure 1A).[18] Similar results were obtained in a second scRNA-seq dataset comprising of melanoma patients treated with immune checkpoint inhibitors (Figure 1B).[19] To complement these findings, we performed double immunofluorescence staining and found that ATX colocalized with myeloid cells in both primary and metastatic human melanoma biopsies (Figure 1C).

Deletion of ATX in LysM+ myeloid cells reduces the number of spontaneous and experimental melanoma lung metastases without affecting primary melanoma growth

To determine whether ATX derived from innate immune cells affects melanoma progression, we conditionally deleted ATX in myeloid lineage cells by crossing Enpp2$^{fl/fl}$ mice with B6.129P2-Lyz2$^{tm1(cre)Ifo}$ mice that express Cre recombinase under the control of the lysozyme 2 promoter (LysM). Knockout (KO) of ATX was verified in myeloid cells purified from the bone marrow of LysM-WT or LysM-KO mice by immunoblot. ATX protein was below detectable levels in LysM-KO cells compared to LysM-WT cells (Figure S1A). As ATX is a secreted enzyme, we also measured the enzyme activity and protein levels in the supernatants of isolated myeloid cells. ATX activity and protein were 70% lower in the supernatant of LysM-KO cells compared to WT cells (Figures S1B and S1C). Interestingly, we observed a 50% reduction of ATX protein in the plasma of LysM-KO mice relative to LysM-WT mice (Figure S1D), indicating that deletion of ATX in LysM+ myeloid cells also reduced the levels of circulating ATX by half.

Using this mouse model, we first investigated the role of myeloid cell-derived ATX in the growth of B16-F10 primary tumors in both male and female mice. TdTB16-F10 cells were injected subcutaneously into LysM-WT and LysM-KO mice of both sexes, and tumor growth was measured on days (D) 4, 7, 9, 11 and 14 post-inoculation (Figure 2A). We observed no differences in the growth rate or size of primary tumors between LysM-WT and LysM-KO mice in both sexes (Figures 2B, 2C, S1E, and S1F). One advantage of using the subcutaneous B16-F10 model is that it emulates the orthotopic spread of melanoma by invading the basement membrane and developing spontaneous lung metastases (i.e., SMM). On D14, the lungs from these mice were removed and examined under a fluorescence microscope to detect spontaneous lung metastases. We found that the number of spontaneous lung metastases was significantly reduced by ~55% in LysM-KO mice compared to LysM-WT mice in both sexes (Figures 2D and S1G; $p < 0.05$). As several publications have reported sex-based differences in immune response to inflammation and cancer, we decided to only conduct our studies in female mice from this point onward.[20–22]

We expanded our observations to include the EMM, another model that is commonly used to study metastatic progression. TdTB16-F10 cells were injected intravenously into LysM-WT and LysM-KO mice. Lungs were excised on D1, D3, D10, and D18 to investigate if deleting ATX in myeloid cells affects the early-, mid-, and/or late-stage metastatic process (Figure 2E). Similar to the results of the SMM, we observed a 50% reduction in the number of lung metastases in LysM-KO mice relative to LysM-WT mice at D10 and D18, but not at D1 or D3 (Figures 2F and 2G; $p < 0.05$ and $p < 0.0001$). These findings suggest that ATX derived from myeloid cells may not alter the initial seeding or arrest of B16-F10 cells in the lungs but has a greater impact on the mid-to late-stage metastatic process.

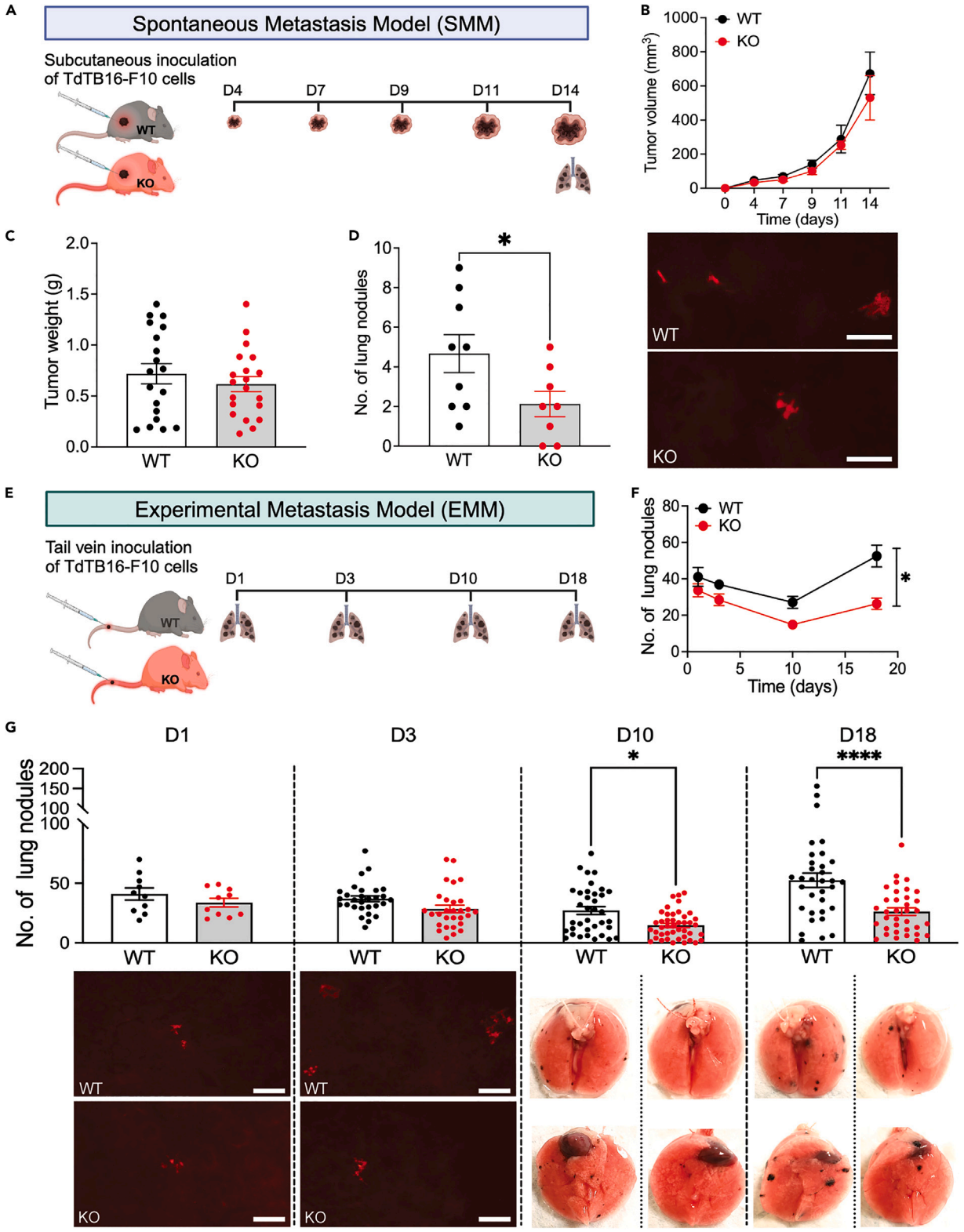

Figure 2. ATX deletion in LysM+ myeloid cells reduced the number of melanoma lung metastatic nodules but had no effect on primary tumor growth

(A) Schematic of spontaneous metastasis model (SMM).

(B) No difference in primary tumor growth (size in mm^3) between LysM-WT and LysM-KO female mice from D0 to D14.

Figure 2. *Continued*

(C) No difference in primary tumor weight (in g) at D14 between the two genotypes.

(D) LysM-KO female mice had 55% fewer spontaneous lung micro-metastases than LysM-WT female mice. The panels on the right of the graph show representative images of lung micro-metastases.

(E) Schematic of experimental metastasis model (EMM). (F and G) The number of metastatic lung nodules in the EMM at D1, D3, D10 and D18 were quantified either by fluorescence microscopy (D1 and D3) or by eye (D10 and D18). No differences were observed in the number of metastatic lung nodules at D1 between LysM-WT and LysM-KO mice. At D3, a 23% reduction in metastatic lung nodules was found in LysM-KO mice but did not achieve statistical significance. At D10 and D18, LysM-KO mice had 50% reduction in the number of metastatic lung nodules compared to LysM-WT mice. White scale bars represent 100 μm. N number of mice is represented by individual black (WT) and red (KO) dots in the graphs. Each group has a minimum of 8 mice per genotype. Statistical analysis was performed using unpaired t-test for (D) and two-way ANOVA with Sidak's multiple comparison test for (F and G). Values with $*p < 0.05$ and $****p < 0.0001$ are considered to be statistically significant. All data shown are mean ± SEM.

LysM-WT mice present increased levels of 18:2- and 20:4-LPA during metastatic progression compared to LysM-KO mice

Heterozygous germline ATX-KO mice possess plasma ATX activity and LPA levels that are half that of WT mice.[23] Conditional KO of ATX in adipocytes leads to a 90% reduction of ATX in white and brown adipose tissue, accompanied by a 38% reduction in levels of plasma LPA.[24] To investigate whether KO of ATX in LysM+ myeloid cells altered plasma LPA levels, we measured the levels of multiple LPA acyl species (16:0-LPA, 18:0-LPA, 18:1-LPA, 18:2-LPA, and 20:4-LPA) in the plasma of LysM-WT and LysM-KO mice under naive conditions (i.e., non-tumor bearing mice) and also at various time points of the SMM and EMM (Figure S2). We found that the total concentration of LPA species to be the same in both genotypes, irrespective of whether the mice had tumors or not (Figure 3A). However, an increase in the plasma concentrations of 18:2-LPA and 20:4-LPA was observed in tumor bearing mice compared to naive mice, with the concentration of these two LPA species being significantly lower in LysM-KO mice than in LysM-WT mice. (Figures 3B and 3C; $p < 0.05$ and $p < 0.01$).

We also examined the levels of pro- and anti-inflammatory cytokines in the plasma of LysM-WT and LysM-KO mice in both SMM and EMM. Out of the 13 cytokines measured, we observed significant decrease in the concentrations of IL-12p70, IL-27, and IL-17A in the plasma of LysM-KO mice compared to LysM-WT mice only at D18 of EMM, but not at D10 (EMM) or D14 (SMM) (Figures 3D, 3E, and 3F; $p < 0.05$). No differences in the levels of the remaining 10 cytokines were observed between the genotypes (Figure S3).

The immune cell landscape in the lungs and spleens differs in tumor-bearing LysM-KO mice

To better understand the cellular mechanisms responsible for the difference in metastatic progression between LysM-WT and LysM-KO mice, we used flow cytometry to profile the immune cell populations present in the lungs and spleens of these mice. The gating strategy to distinguish distinct myeloid, lymphoid, and natural killer (NK) cell populations are shown in Figures S4–S7, with the markers used to identify each immune cell population listed in Table S1. First, we analyzed the populations of immune cells in the lungs of LysM-WT and LysM-KO mice that developed spontaneous metastases. At D14, the lungs of LysM-KO mice had 40% fewer M2-like alveolar macrophages than LysM-WT mice (Figure 4, LUNG D14 SMM panel; $p < 0.05$ for absolute cell numbers). Although a similar trend was observed for cell percentages, it did not reach statistical significance. In contrast, LysM-KO mice bearing experimental metastasis had higher M2-like alveolar macrophages, but fewer neutrophils and Tregs than LysM-WT mice at D10 (Figure 4, LUNG D10 EMM panel; $p < 0.05$, $p < 0.01$ and $p < 0.001$). The decrease in neutrophil numbers in the lungs of LysM-KO mice persisted to D18 (EMM), whereas alterations in M2-like alveolar macrophages and Tregs subsided (Figure 4, LUNG D18 EMM panel; $p < 0.01$ and $p < 0.001$). Although there was no difference in neutrophil counts between LysM-WT versus LysM-KO mice in SMM, the neutrophil counts in the lungs of LysM-WT mice with experimental metastasis were 2-fold higher than those of LysM-WT mice bearing spontaneous metastasis.

Metastasis associated macrophages (MAMs) have been shown to accumulate in the metastatic lungs of tumor-bearing mice and play important roles in metastatic progression.[17,25] We profiled for MAMs using the published[17] markers F4/80^{+}Ly6G^{-}CD11b^{+++}Ly6C$^{-/lo}$ and found that MAMs only accumulated in the lungs of mice at D18 (EMM), but not at D10 (EMM) or D14 (SMM). Specifically, LysM-KO mice had significantly fewer MAMs compared to LysM-WT mice at D18 (Figure 5; $p < 0.05$). We observed no differences between the two genotypes in the levels of other immune cell types measured, including dendritic cells, eosinophils, and NK cells (Figure S8). Of note, we also looked at exhausted CD8^{+} T cells but the cell number for this population was too low to make any reasonable interpretation.

Next, we examined alterations in immune cell population in the spleen. No differences in myeloid cell populations were observed in the spleen of LysM-WT versus LysM-KO mice in SMM (Figure 6, SPLEEN D14 SMM panel). In contrast to the lungs, only alterations in neutrophils were seen in the spleen of mice at D10 throughout D18 of EMM (Figure 6, SPLEEN D10 and D18 EMM panels; $p < 0.01$). Although there appears to be a trend of fewer M2-like Lyc6^{lo} monocytes/macrophages in the spleen of LysM-KO mice at D10, the difference was not statistically significant in terms of absolute numbers. Similar to the lungs, LysM-WT mice with experimental metastasis had higher number of neutrophils in the spleens than LysM-WT mice with spontaneous metastasis.

DISCUSSION

Our initial finding that ATX is abundantly expressed by myeloid cells in human and mouse melanomas prompted us to focus our investigation on the role of ATX in modulating innate tumor immunity. Here, we show that deleting ATX in LysM+ myeloid cells reduces the formation of melanoma metastases but not primary tumor growth. There are conflicting reports in the literature regarding the involvement of ATX in regulating tumor growth. While we and others have demonstrated that pharmacological inhibition of ATX had no effect on the growth of murine

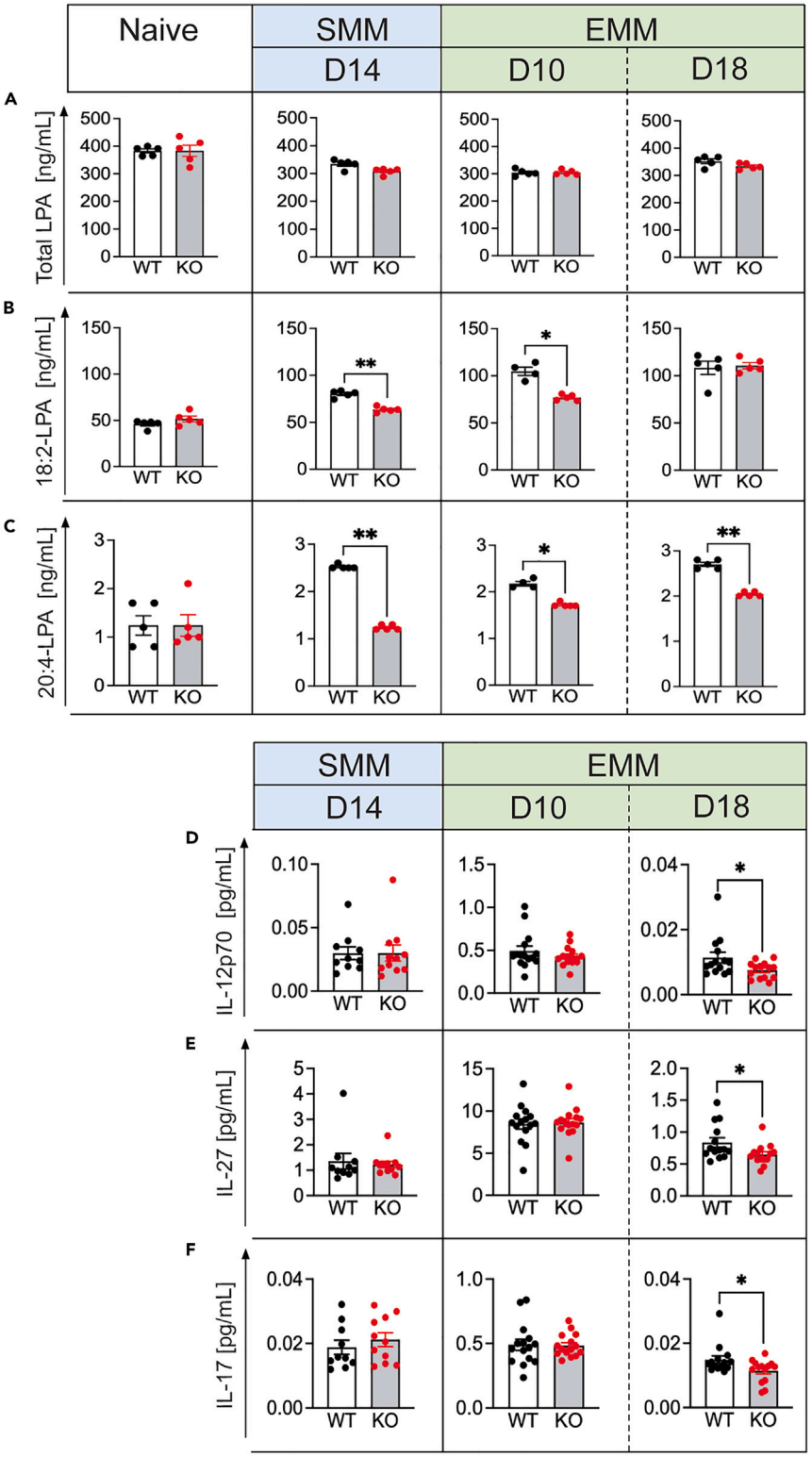

Figure 3. LPA species and cytokine measurements in the plasma of LysM-WT and LysM-KO mice

(A–C) LPA species in EDTA-plasma from naive non-tumor bearing mice, mice from the SMM at D14, or mice from the EMM at D10 or D18 were measured by mass spectrometry. Plasma collected from LysM-WT and LysM-KO mice from 3 independent experiments were pooled for the analyses (WT $n = 10$; KO $n = 10$) and ran as 5 technical replicates. (A) Total plasma LPA levels were the same between LysM-WT and LysM-KO mice under naive conditions, and at the different time points

Figure 3. *Continued*

and metastasis models tested. (B) At D14 and D10, we detected decreased levels of 18:2-LPA in the plasma of LysM-KO mice. (C) At D14, D10, and D18, LysM-KO mice exhibited decreased levels of 20:4-LPA relative to LysM-WT mice. Statistical analysis was performed with Mann-Whitney test where $*p < 0.05$ and $**p < 0.01$. (D–F) Cytokine measurements in plasma from LysM-WT and LysM-KO mice bearing spontaneous or experimental lung metastases ($n = 10$ mice per genotype at minimum). Shown here are measurements for (D) IL-12p70, (E) IL-27, and (F) IL-17, where no changes were observed between the genotypes at D14 and D10. Whereas at D18, levels of all three cytokines were significantly higher in LysM-WT mice compared to LysM-KO. Data shown are mean ± SEM. Statistical analysis was performed with unpaired t-test with $*p < 0.05$.

primary melanoma and lung cancer in mice,[7,26] other studies showed that ATX inhibitors effectively suppress the growth of breast and pancreatic tumors in mice.[27–30] Thus, the effect of ATX on tumor growth appears to vary depending on the type of tumor.

All previous studies, including ours, have consistently shown that inhibiting ATX either by pharmacological interventions or genetic approaches has a more profound impact on metastasis rather than primary tumor growth.[26–29,31,32] Over the past decade, the focus of ATX-LPA research has transitioned from a cancer cell-centric model to a TME-focused view.[33] Cells of the TME that play a significant role in promoting cancer metastasis have emerged as a crucial source of ATX. For example, inhibiting platelet-derived ATX suppressed metastasis of human breast cancer to the bone.[34] Furthermore, we demonstrated that ATX derived from alveolar type-II epithelial pneumocytes reduced the metastasis of melanoma tumors with low ATX expression and not tumors with high ATX expression.[35] Whereas adipocytes are a major producer of ATX in the TME of breast carcinomas,[36–38] deleting ATX in adipocytes had no effect on breast cancer growth and metastasis in mice.[28] In the present study, LysM+ myeloid cells were found to be an important source of ATX and LPA in melanoma and a driver of metastatic progression in mice.

When comparing ATX protein levels in the plasma of LysM-WT and LysM-KO mice, we discovered that circulating ATX levels were 50% lower in LysM-KO mice. However, we found no difference in total plasma LPA levels between the two genotypes under naive conditions. To understand this discrepancy, we examined whether myeloid cells from LysM-WT and LysM-KO mice differed in their expression of membrane-associated phosphatidic acid (PA)-selective phospholipase A_1 (mPA-PLA$_1\alpha$ and mPA-PLA$_1\beta$), which can generate LPA from PA.[39] We found that myeloid cells do not express mPA-PLA$_1\beta$, which is not surprising as mPA-PLA$_1\beta$ has been reported to be expressed exclusively in human testes.[39] The expression of mPA-PLA$_1\alpha$ was increased in CD11b+ myeloid cells from LysM-KO mice compared to LysM-WT mice (Figure S9). However, the extent of mPA-PLA$_1\alpha$ contribution to LPA levels in the plasma has not been investigated before, and its expression has mainly been found in hair follicles.[39] We also looked at the expression of LPP family of enzymes that are known to degrade LPA. Of these, CD11b+ myeloid cells from LysM-KO mice appear to have higher levels of LPP1 and LPP3 transcripts compared to LysM-WT mice. Studies have shown that genetic disruption of LPP1 in mice globally, or specific deletion of LPP3 in liver, moderately elevated plasma LPA levels.[40,41] Our finding that CD11b+ myeloid cells lacking ATX expression have higher mPA-PLA$_1\alpha$, LPP1, and LPP3 expressions could not explain the lack of changes in total plasma LPA levels between LysM-WT and KO mice. To answer these questions, further investigation is needed into additional mechanisms or cell types that could account for the lack of differences in total LPA levels despite a 50% reduction in circulating ATX in LysM-KO mice.

Nonetheless, we found that tumor inoculation increased plasma levels of 18:2- and 20:4-LPA in both LysM-WT and LysM-KO mice. Interestingly, mice with bone cancer exhibit elevated serum levels of 18:1-, 18:2-, and 20:4-LPA, relative to those in naive mice.[42] Similarly, high levels of 20:4-, 18:2-, and 16:0-LPA were detected in the ascites of ovarian cancer patients, where patient-derived TAMs, but not tumor cells, were the primary source of 20:4-LPA in the ascites fluid.[14] Of note, we found that the levels of 18:2- and 20:4-LPA were significantly lower in LysM-KO mice than in LysM-WT mice at D14 (SMM) and D10 (EMM), whereas at D18 (EMM), only the levels of 20:4-LPA were decreased in the KO animals. Thus, it will be of interest to determine whether TAMs isolated from LysM-KO mice produce lower amounts of 18:2- and/or 20:4-LPA.

No significant differences in the circulating levels of 10 pro- and anti-inflammatory cytokines were observed between the two genotypes. Only at D18 (EMM) did we see a slight decrease in the levels of IL-17A, IL12p70, and IL-27 in LysM-KO mice. This was an unexpected finding, as we anticipated greater differences in cytokines given the 50% reduction in metastatic burden in LysM-KO mice. Interestingly, IL-17A and IL-27 are involved in modulating the functions of macrophages, neutrophils, and MDSCs, playing both pro- and anti-tumorigenic roles.[30,43,44] IL-12 exhibits anti-tumor activity and is being explored currently as a target for cancer immunotherapy.[45]

We found that deleting ATX in LysM+ myeloid cells was accompanied by differential changes in the immune cell landscape between SMM versus EMM, and also between the metastatic lungs and spleen. In SMM, fewer M2-like macrophages were found in the lungs of LysM-KO mice compared to LysM-WT mice. Whereas in the EMM, LysM-KO mice had more M2-like alveolar macrophages, but fewer neutrophils and Tregs than LysM-WT mice at D10. However, only neutrophils remained low at D18 (EMM) revealing the dynamic change in the immune landscape as the tumor progresses. Interestingly, we found that MAMs accumulated in the lungs of mice only at D18 (EMM), with LysM-KO mice having fewer MAMs than LysM-WT mice (Figure 5). We hypothesize that MAM accumulation may be more pronounced in late-stage metastasis (D18), when the disease is more advanced. MAMs have been reported to support the growth of breast cancer tumors at the metastatic niche by suppressing the anti-tumor response of cytotoxic $CD8^+$ T cells and NK.[17,25]

The spleen may function as a reservoir for immune cells that can influence tumor progression. In a mouse model of lung adenocarcinoma, tumor-promoting neutrophils have been shown to migrate from the spleen to tumor.[46] In our study, we found no alterations in myeloid cell populations in the spleens of LysM-WT and LysM-KO mice in SMM. In contrast, neutrophil counts were significantly lower in the spleen of LysM-KO mice at D10 throughout D18 in EMM. An interesting observation was that neutrophil counts were higher in both the lungs and spleens of LysM-WT mice bearing experimental metastasis compared to LysM-WT mice bearing spontaneous metastasis. It is possible

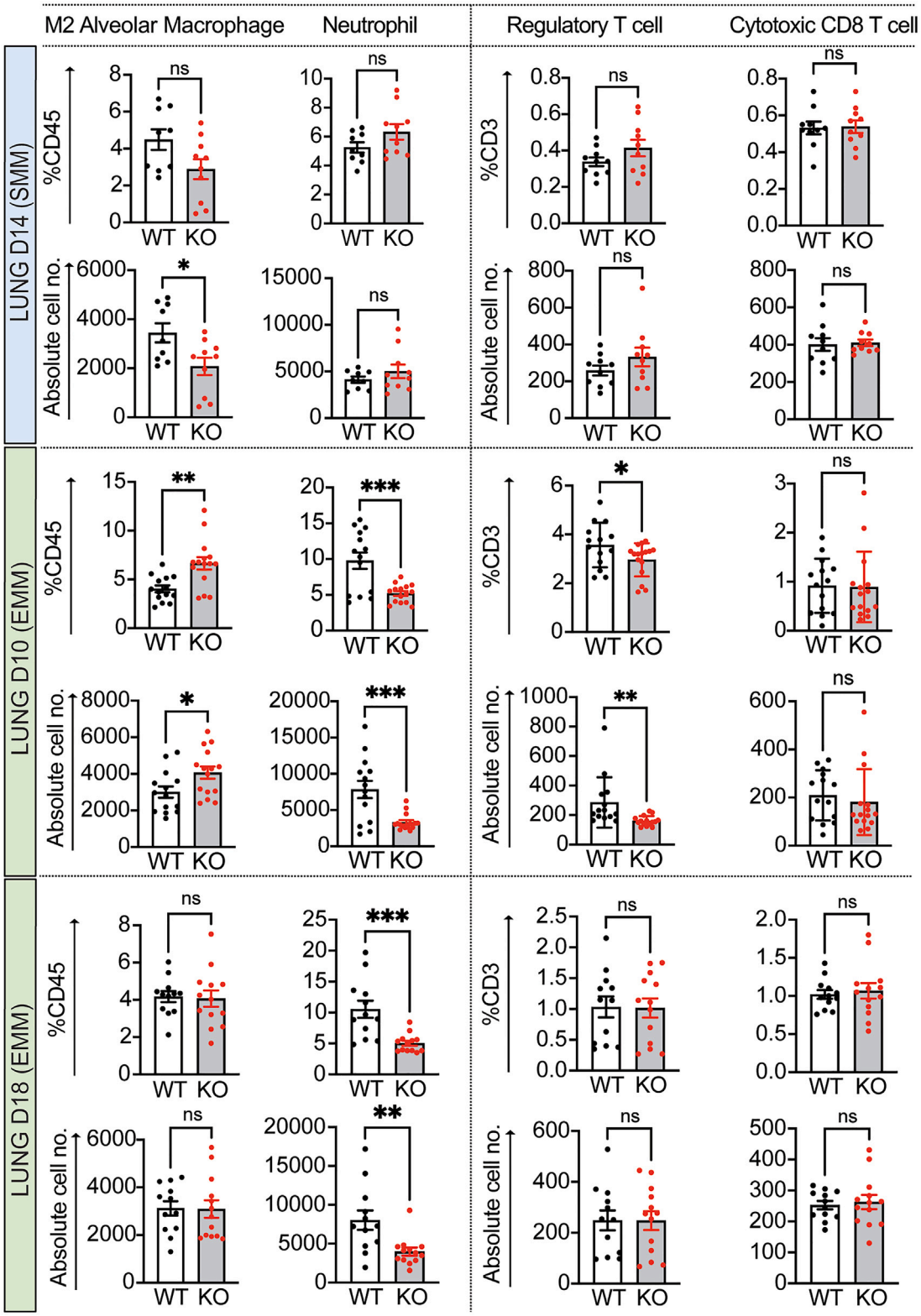

Figure 4. Immune cell profiles in the lungs of LysM-WT and LysM-KO mice from both SMM and EMM

Differences in immune cell populations in the lungs at D14 (Top panel), D10 (Mid panel), and D18 (Bottom panel). Data is expressed as mean of percentages of $CD45^+$ for myeloid population or $CD3^+$ for lymphoid population ±SEM, with corresponding absolute cell number (per 200,000 total viable cells) shown below. N

Figure 4. *Continued*

number of mice is represented by individual black (WT) and red (KO) dots in the graphs. Each group has at least a minimum of 9 mice per genotype. Statistical analysis was performing with unpaired t-test with *$p < 0.05$, **$p < 0.01$, and ***$p < 0.001$ are considered to be statistically significant, whereas values denoted by ns are not.

that neutrophil accumulation may be more pronounced when metastatic nodules are more numerous and developed at D10 and D18 (EMM), compared to D14 (SMM). Another possible reason could be due to the bolus injection of a large number of tumor cells given intravenously in the EMM that may trigger a host response that differs from the gradual invasion of tumor cells from the primary tumor into the circulation. In this regard, a similar finding of neutrophilia in the lungs of mice with experimental melanoma metastasis was recently reported and found to promote metastatic progression.[47] Thus, it would be of interest to study if the increase in neutrophils seen in the metastatic lungs of LysM-WT mice originated from spleen, and whether deleting ATX in neutrophils could impair this process resulting in fewer metastasis in the lungs of LysM-KO mice.

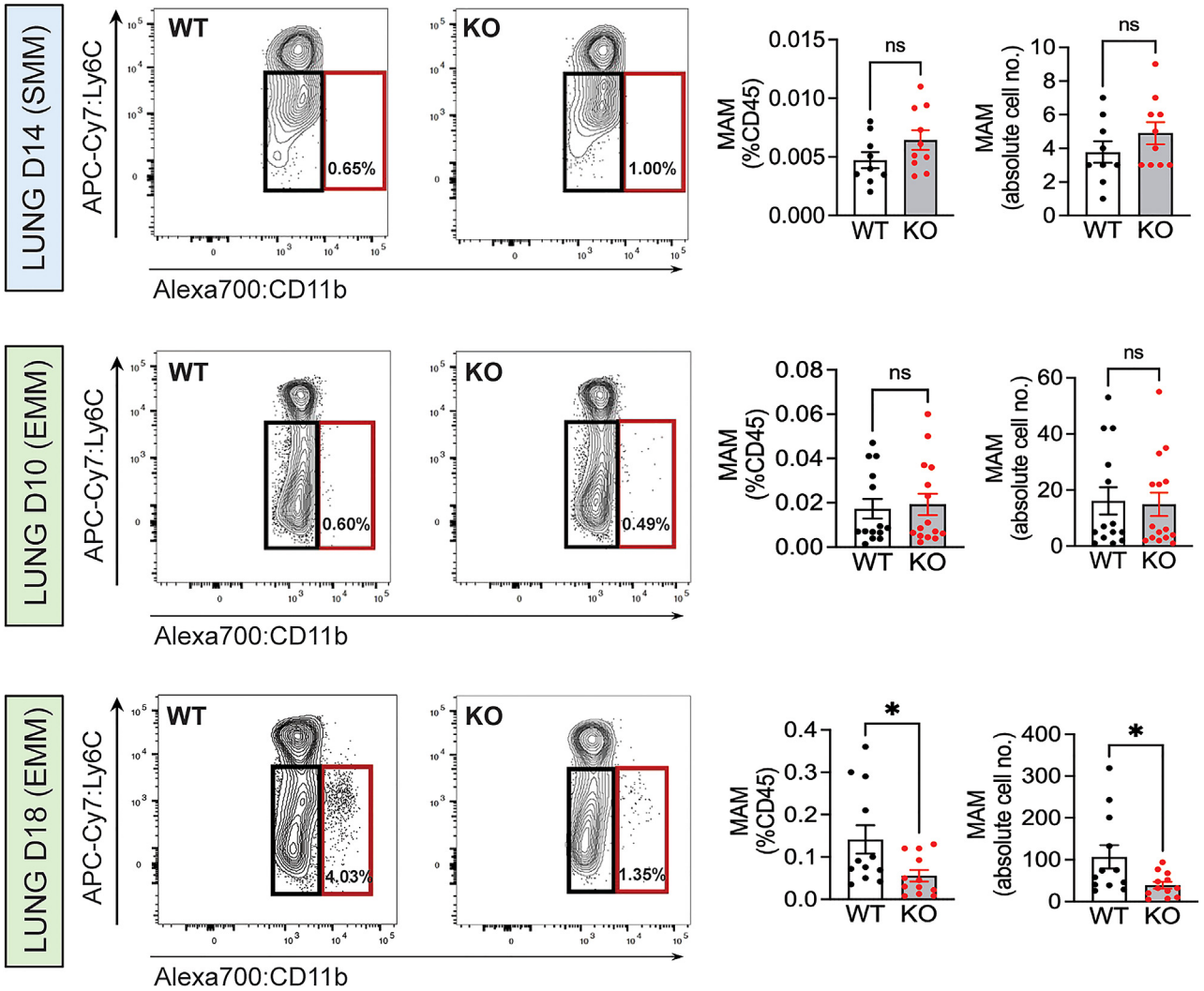

Figure 5. Accumulation of MAM population at D18 (EMM) in LysM-WT mice

After collection and digestion of the lungs, red blood cells were lysed, and the remaining cells were stained and fixed in PBS 2% formalin. Flow cytometry was performed using a 10-color antibody-panel. Dead cells were excluded and live single cells (Zombie Green-) were analyzed for surface expression of CD45. MAM population (red boxes) was identified using the following markers $F480^{+}$ $Ly6G^{-}$ $CD11b^{+++}$ $Ly6C^{-/lo}$. MAM population at D14 (Top panel), D10 (Mid panel), and D18 (Bottom panel). Left panels: representative flow cytometry gating of MAM population. Right panels: MAMs shown as percentages of $CD45^{+}$ cells and absolute cell number (per 200,000 total viable cells). N number of mice is represented by individual black (WT) and red (KO) dots in the graphs. Each group has a minimum of 9 mice per genotype. Statistical analysis performed with unpaired t-test. Data shown as mean ± SEM where *$p < 0.05$ is considered statistically significant.

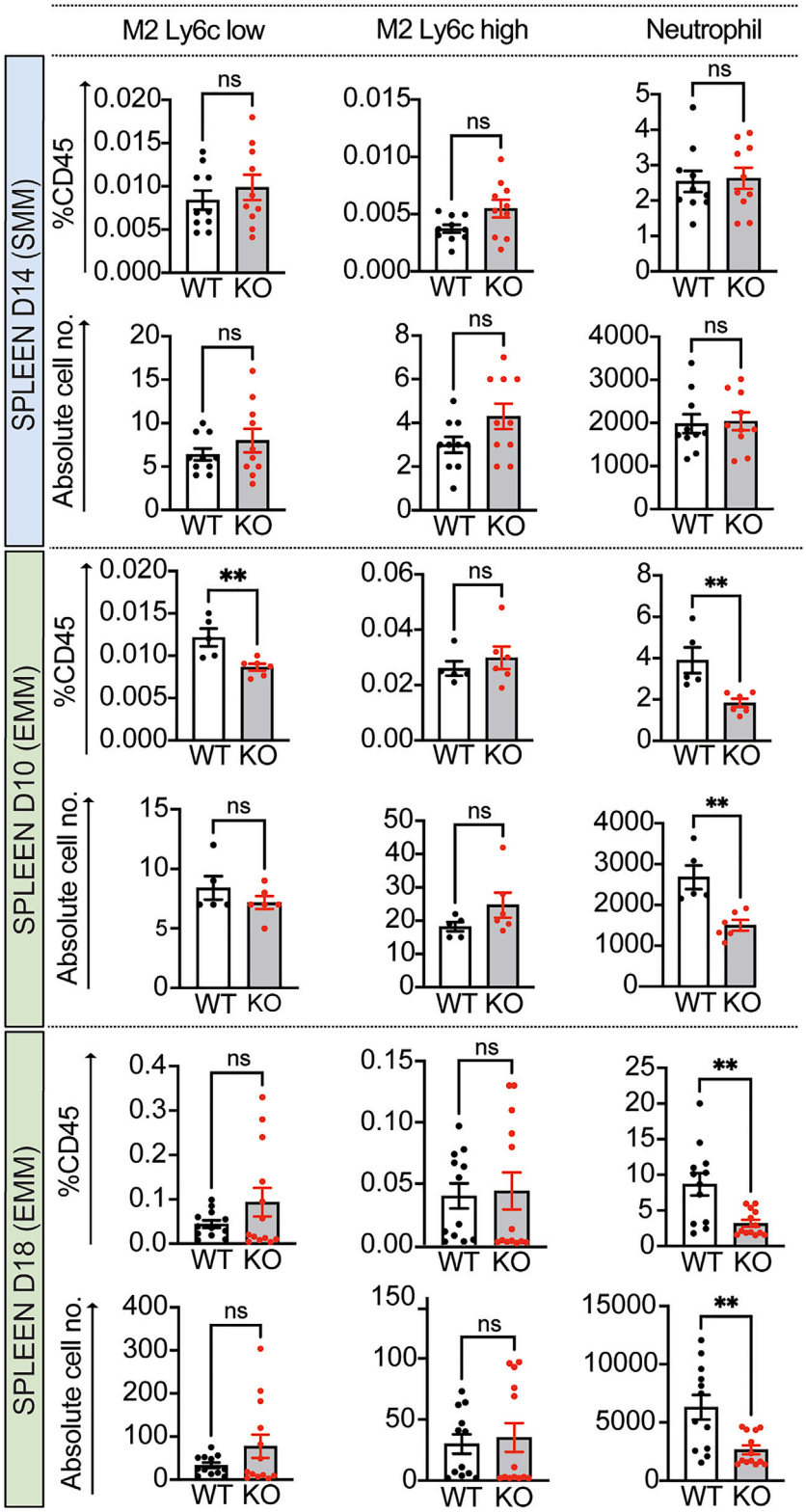
M2 Ly6c low
M2 Ly6c high
Neutrophil
SPLEEN D14 (SMM)
SPLEEN D10 (EMM)
SPLEEN D18 (EMM)
%CD45
Absolute cell no.
WT
KO
ns
**

Figure 6. Immune cell profiles in the spleens of LysM-WT and LysM-KO mice from both SMM and EMM

Differences in immune cell populations in the spleen of LysM-WT and LysM-KO mice at D14 (Top panel), D10 (Mid panel), and D18 (Bottom panel). Data are expressed as mean of percentages of $CD45^+$ cells ±SEM, with the corresponding absolute cell number (per 100,000 total viable cells) shown below. N number of mice is represented by individual black (WT) and red (KO) dots in the graphs. Each group has a minimum of 5 mice per genotype. Statistical analysis was performed with unpaired t-test where $^{**}p < 0.01$ is considered to be statistically significant, whereas values denoted by ns are not.

Although not in the context of cancer, several studies have reported that LPA promotes neutrophil polarization and motility.[48–50] Moreover, ATX expression is found in close proximity to neutrophil extracellular traps (NETs) in human pulmonary thrombus biopsies, and that LPA treatment of human neutrophils induces the formation of NETs *in vitro*.[51] In contrast, a recent study reported that activation of LPAR3 by LPA suppresses the formation of NETs in a mouse model of sepsis.[52] In terms of macrophage function, studies have reported that LPA induces differentiation of human $CD34^+$ stem cells to myeloid cells and converts mouse and human monocytes to macrophages via activation of PPARγ.[53,54] LPA-mediated Akt/mTOR signaling is also critical for macrophage development in mice.[54] In contrast, the loss of ATX expression in LysM+ myeloid cells impairs toll-like receptor 4 (TLR4) signaling and disrupts the phagocytic function of macrophages, thereby increasing the severity of inflammatory bowel disease.[55] These studies highlight a gap in our knowledge of how ATX and LPA modulate neutrophil and macrophage function in cancer.

Lastly, although EMM is useful for studying the early to late stages of the metastatic cascade, especially when modeling tumors that show long latency in developing spontaneous metastases, it does not recapitulate two critical processes of the metastatic cascade: (1) the extravasation of cancer cells from the primary tumor into the circulation and (2) the establishment of a premetastatic niche, which is aided in part by secreted factors produced by the primary tumor.[56] Thus, the differences in the immune cell profiles between the two metastatic models that we observed in our current study could be attributed to this. Furthermore, intratumor heterogeneity can diverge in metastatic tumors that arise spontaneously versus those induced experimentally, which could influence the immune landscape of the TME.[57,58]

In summary, we show that ATX derived from LysM+ myeloid cells can regulate innate anti-tumor responses to promote metastasis of melanoma to the lung. Our findings extend the immunomodulatory functions of ATX-LPA from adaptive to innate tumor immunity, making this signaling pathway a viable therapeutic target for cancer immunotherapy. Additionally, immunological snapshots taken at various stages of tumor progression reveal dynamic changes in the anti-tumor immune response that will have to be taken into consideration in the study design of subsequent metastasis models.

Limitations of the study

We acknowledge that our current study has several limitations. First, we did not resect the subcutaneous primary tumor to allow for spontaneous micro-metastases to progress to advanced late-stage metastases and compare the results to those of the EMM. Despite this, the observation that deleting ATX in LysM+ myeloid cells reduced both spontaneous and experimental metastases suggests that ATX derived from myeloid cells serves as an important regulator of innate tumor immunity that controls metastatic progression. Second, the specificity of LysM-Cre is not limited to macrophages and neutrophils only. Publication by the Jackson Laboratory showed that LysM is expressed by 60–80% of neutrophils in spleen, peripheral blood, and bone marrow. About 90–100% of alveolar or peritoneal macrophages express LysM, whereas only 40% of mature macrophages in spleen were LysM positive. In addition, a minor population of CD11c+ dendritic cells, as well as alveolar type-II epithelial pneumocytes in mice also expresses LysM.[59] This is one of the reasons why we performed a comprehensive immunoprofiling that includes neutrophils, eosinophils, dendritic cells, monocytes, and macrophages in order to account for differences that may arise in these cell populations as a result of LysM-Cre mediated ATX deletion. The contribution of ATX from alveolar type-II epithelial pneumocytes on melanoma metastasis has been addressed in our previous publication, where ATX produced from these cells affects the metastasis of melanoma tumors with low ATX expression rather than tumors with high ATX expression.[35] Third, the mechanism by which ATX-deleted macrophages and neutrophils suppress melanoma lung metastasis warrants further investigation.

RESOURCE AVAILABILITY

Lead contact

Further information and requests for resources and reagents should be directed to and will be fulfilled by the lead contact, Sue Chin Lee (slee84@uthsc.edu).

Materials availability

This study did not generate new unique reagents.

Data and code availability

- Raw western blot images have been uploaded and publicly available at Mendeley Data https://doi.org/10.17632/td7h8w9s32.1.
- All data reported in this paper will be shared by the lead contact upon request.
- This paper does not report original code.

ACKNOWLEDGMENTS

This work was supported by grants from NCI CA092160-18 (G.J.T.), NCI CA266207-01A1 (G.J.T. and S.C.L.), the William and Ella Owens Foundation (S.C.L.), the Harriett Van Vleet Endowment in Basic Oncology Research (G.J.T.), the UTHSC Office of Research CORNET Grant (S.C.L.) and by gift of Dr. Joseph Tarnowski,

PhD, to UT Foundation to finance Independent Project Grant from the College of Graduate Health Sciences of UTHSC (M.A.D.). The authors wish to thank Dr. Louisa Balazs, MD, PhD, for her assistance with the histopathology and immune histology review of our cases, Dr. Kyle Johnson Moore, PhD, in the UTHSC Office of Scientific Writing for editing the manuscript, Dr. Deidre Daria, PhD, from the UTHSC Flow cytometry Core for her help with the flow cytometry analyses and Prof. Raul Torres, PhD, for critical reading and advice of the manuscript. Graphical abstract was generated using Biorender.com.

AUTHOR CONTRIBUTIONS

Conceptualization, M.A.D., D.D.N., G.J.T., and S.C.L.; methodology, M.A.D., D.D.N., G.J.T., and S.C.L.; investigation, M.A.D., D.D.N., Y.S., and S.C.L.; validation, M.A.D., D.D.N., Y.S., and S.C.L.; formal analysis, M.A.D., D.D.N., G.J.T., and S.C.L.; writing—review and editing, M.A.D., D.D.N., G.J.T., and S.C.L.; visualization, M.A.D. and S.C.L.; funding acquisition, M.A.D., G.J.T., and S.C.L.

DECLARATION OF INTERESTS

The authors declare no conflict of interest.

STAR★METHODS

Detailed methods are provided in the online version of this paper and include the following:

- KEY RESOURCES TABLE
- EXPERIMENTAL MODELS AND HUMAN MATERIALS
  - Human materials
  - *In vivo* mouse models
  - Melanoma cell lines
- METHOD DETAILS
  - Sample collection
  - Spontaneous and experimental metastasis models
  - Immunoblot analysis
  - Histology and immunostaining of human samples
  - T-SNE plots
  - Flow cytometry
  - Measurement of ATX activity
  - LPA quantification
  - Measurement of cytokines
  - Real-time quantitative PCR (RT-qPCR)
- QUANTIFICATION AND STATISTICAL ANALYSIS

SUPPLEMENTAL INFORMATION

Supplemental information can be found online at https://doi.org/10.1016/j.isci.2024.110971.

Received: February 8, 2024
Revised: August 4, 2024
Accepted: September 13, 2024
Published: September 17, 2024

REFERENCES

1. Lee, D., Suh, D.S., Lee, S.C., Tigyi, G.J., and Kim, J.H. (2018). Role of autotaxin in cancer stem cells. Cancer Metastasis Rev. *37*, 509–518. https://doi.org/10.1007/s10555-018-9745-x.
2. Lee, S.C., Dacheux, M.A., Norman, D.D., Balázs, L., Torres, R.M., Augelli-Szafran, C.E., and Tigyi, G.J. (2020). Regulation of Tumor Immunity by Lysophosphatidic Acid. Cancers *12*, 1202. https://doi.org/10.3390/cancers12051202.
3. Kano, K., Aoki, J., and Hla, T. (2022). Lysophospholipid Mediators in Health and Disease. Annu. Rev. Pathol. *17*, 459–483. https://doi.org/10.1146/annurev-pathol-050420-025929.
4. Leblanc, R., and Peyruchaud, O. (2015). New insights into the autotaxin/LPA axis in cancer development and metastasis. Exp. Cell Res. *333*, 183–189. https://doi.org/10.1016/j.yexcr.2014.11.010.
5. Altman, M.K., Gopal, V., Jia, W., Yu, S., Hall, H., Mills, G.B., McGinnis, A.C., Bartlett, M.G., Jiang, G., Madan, D., et al. (2010). Targeting melanoma growth and viability reveals dualistic functionality of the phosphonothionate analogue of carba cyclic phosphatidic acid. Mol. Cancer *9*, 140. https://doi.org/10.1186/1476-4598-9-140.
6. Turner, J.A., Fredrickson, M.A., D'Antonio, M., Katsnelson, E., MacBeth, M., Van Gulick, R., Chimed, T.S., McCarter, M., D'Alessandro, A., Robinson, W.A., et al. (2023). Lysophosphatidic acid modulates CD8 T cell immunosurveillance and metabolism to impair anti-tumor immunity. Nat. Commun. *14*, 3214. https://doi.org/10.1038/s41467-023-38933-4.
7. Konen, J.M., Rodriguez, B.L., Wu, H., Fradette, J.J., Gibson, L., Diao, L., Wang, J., Schmidt, S., Wistuba, I.I., Zhang, J., and Gibbons, D.L. (2023). Autotaxin suppresses cytotoxic T cells via LPAR5 to promote anti-PD-1 resistance in non-small cell lung cancer. J. Clin. Invest. *133*, e163128. https://doi.org/10.1172/JCI163128.
8. Matas-Rico, E., Frijlink, E., van der Haar Àvila, I., Menegakis, A., van Zon, M., Morris, A.J., Koster, J., Salgado-Polo, F., de Kivit, S., Lança, T., et al. (2021). Autotaxin impedes anti-tumor immunity by suppressing chemotaxis and tumor infiltration of CD8(+) T cells. Cell Rep. *37*, 110013. https://doi.org/10.1016/j.celrep.2021.110013.
9. Oda, S.K., Strauch, P., Fujiwara, Y., Al-Shami, A., Oravecz, T., Tigyi, G., Pelanda, R., and Torres, R.M. (2013). Lysophosphatidic acid inhibits CD8 T cell activation and control of tumor progression. Cancer Immunol. Res. *1*, 245–255. https://doi.org/10.1158/2326-6066.CIR-13-0043-T.
10. Mathew, D., Kremer, K.N., Strauch, P., Tigyi, G., Pelanda, R., and Torres, R.M. (2019). LPA(5) Is an Inhibitory Receptor That Suppresses CD8 T-Cell Cytotoxic Function via Disruption of Early TCR Signaling. Front. Immunol. *10*, 1159. https://doi.org/10.3389/fimmu.2019.01159.
11. Kremer, K.N., Buser, A., Thumkeo, D., Narumiya, S., Jacobelli, J., Pelanda, R., and Torres, R.M. (2022). LPA suppresses T cell function by altering the cytoskeleton and disrupting immune synapse formation. Proc. Natl. Acad. Sci. USA *119*, e2118816119. https://doi.org/10.1073/pnas.2118816119.
12. Chaib, M., Chauhan, S.C., and Makowski, L. (2020). Friend or Foe? Recent Strategies to Target Myeloid Cells in Cancer. Front. Cell

Dev. Biol. *8*, 351. https://doi.org/10.3389/fcell.2020.00351.

13. Wang, Y., Johnson, K.C.C., Gatti-Mays, M.E., and Li, Z. (2022). Emerging strategies in targeting tumor-resident myeloid cells for cancer immunotherapy. J. Hematol. Oncol. *15*, 118. https://doi.org/10.1186/s13045-022-01335-y.
14. Reinartz, S., Lieber, S., Pesek, J., Brandt, D.T., Asafova, A., Finkernagel, F., Watzer, B., Nockher, W.A., Nist, A., Stiewe, T., et al. (2019). Cell type-selective pathways and clinical associations of lysophosphatidic acid biosynthesis and signaling in the ovarian cancer microenvironment. Mol. Oncol. *13*, 185–201. https://doi.org/10.1002/1878-0261.12396.
15. Magkrioti, C., Oikonomou, N., Kaffe, E., Mouratis, M.A., Xylourgidis, N., Barbayianni, I., Megadoukas, P., Harokopos, V., Valavanis, C., Chun, J., et al. (2018). The Autotaxin-Lysophosphatidic Acid Axis Promotes Lung Carcinogenesis. Cancer Res. *78*, 3634–3644. https://doi.org/10.1158/0008-5472.CAN-17-3797.
16. Bhattacharyya, S., Oon, C., Diaz, L., Sandborg, H., Stempinski, E.S., Saoi, M., Morgan, T.K., López, C.S., Cross, J.R., and Sherman, M.H. (2024). Autotaxin-lysolipid signaling suppresses a CCL11-eosinophil axis to promote pancreatic cancer progression. Nat. Can. (Ott.) *5*, 283–298. https://doi.org/10.1038/s43018-023-00703-y.
17. Kitamura, T., Doughty-Shenton, D., Cassetta, L., Fragkogianni, S., Brownlie, D., Kato, Y., Carragher, N., and Pollard, J.W. (2017). Monocytes Differentiate to Immune Suppressive Precursors of Metastasis-Associated Macrophages in Mouse Models of Metastatic Breast Cancer. Front. Immunol. *8*, 2004. https://doi.org/10.3389/fimmu.2017.02004.
18. Jerby-Arnon, L., Shah, P., Cuoco, M.S., Rodman, C., Su, M.J., Melms, J.C., Leeson, R., Kanodia, A., Mei, S., Lin, J.R., et al. (2018). A Cancer Cell Program Promotes T Cell Exclusion and Resistance to Checkpoint Blockade. Cell *175*, 984–997.e24. https://doi.org/10.1016/j.cell.2018.09.006.
19. Sade-Feldman, M., Yizhak, K., Bjorgaard, S.L., Ray, J.P., de Boer, C.G., Jenkins, R.W., Lieb, D.J., Chen, J.H., Frederick, D.T., Barzily-Rokni, M., et al. (2018). Defining T Cell States Associated with Response to Checkpoint Immunotherapy in Melanoma. Cell *175*, 998–1013.e20. https://doi.org/10.1016/j.cell.2018.10.038.
20. Lee, J., Nicosia, M., Hong, E.S., Silver, D.J., Li, C., Bayik, D., Watson, D.C., Lauko, A., Kay, K.E., Wang, S.Z., et al. (2023). Sex-Biased T-cell Exhaustion Drives Differential Immune Responses in Glioblastoma. Cancer Discov. *13*, 2090–2105. https://doi.org/10.1158/2159-8290.CD-22-0869.
21. Kim, M., Lu, R.J., and Benayoun, B.A. (2022). Single-cell RNA-seq of primary bone marrow neutrophils from female and male adult mice. Sci. Data *9*, 442. https://doi.org/10.1038/s41597-022-01544-7.
22. Kay, E., Gomez-Garcia, L., Woodfin, A., Scotland, R.S., and Whiteford, J.R. (2015). Sexual dimorphisms in leukocyte trafficking in a mouse peritonitis model. J. Leukoc. Biol. *98*, 805–817. https://doi.org/10.1189/jlb.3A1214-601RR.
23. van Meeteren, L.A., Ruurs, P., Stortelers, C., Bouwman, P., van Rooijen, M.A., Pradère, J.P., Pettit, T.R., Wakelam, M.J.O., Saulnier-Blache, J.S., Mummery, C.L., et al. (2006). Autotaxin, a secreted lysophospholipase D, is essential for blood vessel formation during development. Mol. Cell Biol. *26*, 5015–5022. https://doi.org/10.1128/MCB.02419-05.
24. Dusaulcy, R., Rancoule, C., Grès, S., Wanecq, E., Colom, A., Guigné, C., van Meeteren, L.A., Moolenaar, W.H., Valet, P., and Saulnier-Blache, J.S. (2011). Adipose-specific disruption of autotaxin enhances nutritional fattening and reduces plasma lysophosphatidic acid. J. Lipid Res. *52*, 1247–1255. https://doi.org/10.1194/jlr.M014985.
25. Brownlie, D., Doughty-Shenton, D., Yh Soong, D., Nixon, C., O Carragher, N., M Carlin, L., and Kitamura, T. (2021). Metastasis-associated macrophages constrain antitumor capability of natural killer cells in the metastatic site at least partially by membrane bound transforming growth factor beta. J. Immunother. Cancer *9*, e001740. https://doi.org/10.1136/jitc-2020-001740.
26. Gotoh, M., Fujiwara, Y., Yue, J., Liu, J., Lee, S., Fells, J., Uchiyama, A., Murakami-Murofushi, K., Kennel, S., Wall, J., et al. (2012). Controlling cancer through the autotaxin-lysophosphatidic acid receptor axis. Biochem. Soc. Trans. *40*, 31–36. https://doi.org/10.1042/BST20110608.
27. Benesch, M.G.K., Tang, X., Maeda, T., Ohhata, A., Zhao, Y.Y., Kok, B.P.C., Dewald, J., Hitt, M., Curtis, J.M., McMullen, T.P.W., and Brindley, D.N. (2014). Inhibition of autotaxin delays breast tumor growth and lung metastasis in mice. Faseb. J. *28*, 2655–2666. https://doi.org/10.1096/fj.13-248641.
28. Tang, X., Morris, A.J., Deken, M.A., and Brindley, D.N. (2023). Autotaxin Inhibition with IOA-289 Decreases Breast Tumor Growth in Mice Whereas Knockout of Autotaxin in Adipocytes Does Not. Cancers *15*, 2937. https://doi.org/10.3390/cancers15112937.
29. Deken, M.A., Niewola-Staszkowska, K., Peyruchaud, O., Mikulčić, N., Antolić, M., Shah, P., Cheasty, A., Tagliavini, A., Nizzardo, A., Pergher, M., et al. (2023). Characterization and translational development of IOA-289, a novel autotaxin inhibitor for the treatment of solid tumors. Immunooncol. Technol. *18*, 100384. https://doi.org/10.1016/j.iotech.2023.100384.
30. Auciello, F.R., Bulusu, V., Oon, C., Tait-Mulder, J., Berry, M., Bhattacharyya, S., Tumanov, S., Allen-Petersen, B.L., Link, J., Kendsersky, N.D., et al. (2019). A Stromal Lysolipid-Autotaxin Signaling Axis Promotes Pancreatic Tumor Progression. Cancer Discov. *9*, 617–627. https://doi.org/10.1158/2159-8290.CD-18-1212.
31. David, M., Wannecq, E., Descotes, F., Jansen, S., Deux, B., Ribeiro, J., Serre, C.M., Grès, S., Bendriss-Vermare, N., Bollen, M., et al. (2010). Cancer cell expression of autotaxin controls bone metastasis formation in mouse through lysophosphatidic acid-dependent activation of osteoclasts. PLoS One *5*, e9741. https://doi.org/10.1371/journal.pone.0009741.
32. Gupte, R., Patil, R., Liu, J., Wang, Y., Lee, S.C., Fujiwara, Y., Fells, J., Bolen, A.L., Emmons-Thompson, K., Yates, C.R., et al. (2011). Benzyl and naphthalene methylphosphonic acid inhibitors of autotaxin with anti-invasive and anti-metastatic activity. ChemMedChem *6*, 922–935. https://doi.org/10.1002/cmdc.201000425.
33. Lee, S.C., Fujiwara, Y., Liu, J., Yue, J., Shimizu, Y., Norman, D.D., Wang, Y., Tsukahara, R., Szabo, E., Patil, R., et al. (2015). Autotaxin and LPA1 and LPA5 receptors exert disparate functions in tumor cells versus the host tissue microenvironment in melanoma invasion and metastasis. Mol. Cancer Res. *13*, 174–185. https://doi.org/10.1158/1541-7786.MCR-14-0263.
34. Leblanc, R., Lee, S.C., David, M., Bordet, J.C., Norman, D.D., Patil, R., Miller, D., Sahay, D., Ribeiro, J., Clézardin, P., et al. (2014). Interaction of platelet-derived autotaxin with tumor integrin alphaVbeta3 controls metastasis of breast cancer cells to bone. Blood *124*, 3141–3150. https://doi.org/10.1182/blood-2014-04-568683.
35. Dacheux, M.A., Lee, S.C., Shin, Y., Norman, D.D., Lin, K.H., E, S., Yue, J., Benyó, Z., and Tigyi, G.J. (2022). Prometastatic Effect of ATX Derived from Alveolar Type II Pneumocytes and B16-F10 Melanoma Cells. Cancers *14*, 1586. https://doi.org/10.3390/cancers14061586.
36. Benesch, M.G.K., Tang, X., Dewald, J., Dong, W.F., Mackey, J.R., Hemmings, D.G., McMullen, T.P.W., and Brindley, D.N. (2015). Tumor-induced inflammation in mammary adipose tissue stimulates a vicious cycle of autotaxin expression and breast cancer progression. Faseb. J. *29*, 3990–4000. https://doi.org/10.1096/fj.15-274480.
37. Volden, P.A., Skor, M.N., Johnson, M.B., Singh, P., Patel, F.N., McClintock, M.K., Brady, M.J., and Conzen, S.D. (2016). Mammary Adipose Tissue-Derived Lysophospholipids Promote Estrogen Receptor-Negative Mammary Epithelial Cell Proliferation. Cancer Prev. Res. *9*, 367–378. https://doi.org/10.1158/1940-6207.CAPR-15-0107.
38. Schmid, R., Wolf, K., Robering, J.W., Strauß, S., Strissel, P.L., Strick, R., Rübner, M., Fasching, P.A., Horch, R.E., Kremer, A.E., et al. (2018). ADSCs and adipocytes are the main producers in the autotaxin-lysophosphatidic acid axis of breast cancer and healthy mammary tissue *in vitro*. BMC Cancer *18*, 1273. https://doi.org/10.1186/s12885-018-5166-z.
39. Yaginuma, S., Kawana, H., and Aoki, J. (2022). Current Knowledge on Mammalian Phospholipase A(1), Brief History, Structures, Biochemical and Pathophysiological Roles. Molecules *27*, 2487. https://doi.org/10.3390/molecules27082487.
40. Tomsig, J.L., Snyder, A.H., Berdyshev, E.V., Skobeleva, A., Mataya, C., Natarajan, V., Brindley, D.N., and Lynch, K.R. (2009). Lipid phosphate phosphohydrolase type 1 (LPP1) degrades extracellular lysophosphatidic acid *in vivo*. Biochem. J. *419*, 611–618. https://doi.org/10.1042/BJ20081888.
41. Busnelli, M., Manzini, S., Hilvo, M., Parolini, C., Ganzetti, G.S., Dellera, F., Ekroos, K., Jänis, M., Escalante-Alcalde, D., Sirtori, C.R., et al. (2017). Liver-specific deletion of the Plpp3 gene alters plasma lipid composition and worsens atherosclerosis in apoE(-/-) mice. Sci. Rep. *7*, 44503. https://doi.org/10.1038/srep44503.
42. Khasabova, I.A., Khasabov, S.G., Johns, M., Juliette, J., Zheng, A., Morgan, H., Flippen, A., Allen, K., Golovko, M.Y., Golovko, S.A., et al. (2023). Exosome-associated lysophosphatidic acid signaling contributes to cancer pain. Pain *164*, 2684–2695. https://doi.org/10.1097/j.pain.0000000000002967.
43. Kuen, D.S., Kim, B.S., and Chung, Y. (2020). IL-17-Producing Cells in Tumor Immunity: Friends or Foes? Immune Netw. *20*, e6. https://doi.org/10.4110/in.2020.20.e6.

44. Ma, S., Cheng, Q., Cai, Y., Gong, H., Wu, Y., Yu, X., Shi, L., Wu, D., Dong, C., and Liu, H. (2014). IL-17A produced by gammadelta T cells promotes tumor growth in hepatocellular carcinoma. Cancer Res. *74*, 1969–1982. https://doi.org/10.1158/0008-5472.CAN-13-2534.
45. Jones, D.S., 2nd, Nardozzi, J.D., Sackton, K.L., Ahmad, G., Christensen, E., Ringgaard, L., Chang, D.K., Jaehger, D.E., Konakondla, J.V., Wiinberg, M., et al. (2022). Cell surface-tethered IL-12 repolarizes the tumor immune microenvironment to enhance the efficacy of adoptive T cell therapy. Sci. Adv. *8*, eabi8075. https://doi.org/10.1126/sciadv.abi8075.
46. Cortez-Retamozo, V., Etzrodt, M., Newton, A., Rauch, P.J., Chudnovskiy, A., Berger, C., Ryan, R.J.H., Iwamoto, Y., Marinelli, B., Gorbatov, R., et al. (2012). Origins of tumor-associated macrophages and neutrophils. Proc. Natl. Acad. Sci. USA *109*, 2491–2496. https://doi.org/10.1073/pnas.1113744109.
47. Sandri, S., Hebeda, C.B., Broering, M.F., de Paula Silva, M., Moredo, L.F., de Barros E Silva, M.J., Sapata Molina, A., Lopes Pinto, C.A., Duprat Neto, J.P., Reutelingsperger, C.P., et al. (2023). Role of Annexin A1 Secreted by Neutrophils in Melanoma Metastasis. Cells *12*, 425. https://doi.org/10.3390/cells12030425.
48. Chettibi, S., Lawrence, A.J., Stevenson, R.D., and Young, J.D. (1994). Effect of lysophosphatidic acid on motility, polarisation and metabolic burst of human neutrophils. FEMS Immunol. Med. Microbiol. *8*, 271–281. https://doi.org/10.1111/j.1574-695X.1994.tb00452.x.
49. Fischer, L.G., Bremer, M., Coleman, E.J., Conrad, B., Krumm, B., Gross, A., Hollmann, M.W., Mandell, G., and Durieux, M.E. (2001). Local anesthetics attenuate lysophosphatidic acid-induced priming in human neutrophils. Anesth. Analg. *92*, 1041–1047. https://doi.org/10.1097/00000539-200104000-00044.
50. Zhao, C., Sardella, A., Chun, J., Poubelle, P.E., Fernandes, M.J., and Bourgoin, S.G. (2011). TNF-alpha promotes LPA1- and LPA3-mediated recruitment of leukocytes *in vivo* through CXCR2 ligand chemokines. J. Lipid Res. *52*, 1307–1318. https://doi.org/10.1194/jlr.M008045.
51. Li, T., Peng, R., Wang, F., Hua, L., Liu, S., Han, Z., Pei, J., Pei, S., Zhao, Z., Jiang, X., and Chen, X. (2020). Lysophosphatidic acid promotes thrombus stability by inducing rapid formation of neutrophil extracellular traps: A new mechanism of thrombosis. J. Thromb. Haemostasis *18*, 1952–1964. https://doi.org/10.1111/jth.14839.
52. Pei, S., Xu, C., Pei, J., Bai, R., Peng, R., Li, T., Zhang, J., Cong, X., Chun, J., Wang, F., and Chen, X. (2022). Lysophosphatidic Acid Receptor 3 Suppress Neutrophil Extracellular Traps Production and Thrombosis During Sepsis. Front. Immunol. *13*, 844781. https://doi.org/10.3389/fimmu.2022.844781.
53. Evseenko, D., Latour, B., Richardson, W., Corselli, M., Sahaghian, A., Cardinal, S., Zhu, Y., Chan, R., Dunn, B., and Crooks, G.M. (2013). Lysophosphatidic acid mediates myeloid differentiation within the human bone marrow microenvironment. PLoS One *8*, e63718. https://doi.org/10.1371/journal.pone.0063718.
54. Ray, R., and Rai, V. (2017). Lysophosphatidic acid converts monocytes into macrophages in both mice and humans. Blood *129*, 1177–1183. https://doi.org/10.1182/blood-2016-10-743757.
55. Kim, S.J., Howe, C., Mitchell, J., Choo, J., Powers, A., Oikonomopoulos, A., Pothoulakis, C., Hommes, D.W., Im, E., and Rhee, S.H. (2020). Autotaxin loss accelerates intestinal inflammation by suppressing TLR4-mediated immune responses. EMBO Rep. *21*, e49332. https://doi.org/10.15252/embr.201949332.
56. Francia, G., Cruz-Munoz, W., Man, S., Xu, P., and Kerbel, R.S. (2011). Mouse models of advanced spontaneous metastasis for experimental therapeutics. Nat. Rev. Cancer *11*, 135–141. https://doi.org/10.1038/nrc3001.
57. Serrano, A., Weber, T., Berthelet, J., El-Saafin, F., Gadipally, S., Charafe-Jauffret, E., Ginestier, C., Mariadason, J.M., Oakes, S.R., Britt, K., et al. (2023). Experimental and spontaneous metastasis assays can result in divergence in clonal architecture. Commun. Biol. *6*, 821. https://doi.org/10.1038/s42003-023-05167-5.
58. Sprouffske, K., Kerr, G., Li, C., Prahallad, A., Rebmann, R., Waehle, V., Naumann, U., Bitter, H., Jensen, M.R., Hofmann, F., et al. (2020). Genetic heterogeneity and clonal evolution during metastasis in breast cancer patient-derived tumor xenograft models. Comput. Struct. Biotechnol. J. *18*, 323–331. https://doi.org/10.1016/j.csbj.2020.01.008.
59. Shi, J., Hua, L., Harmer, D., Li, P., and Ren, G. (2018). Cre Driver Mice Targeting Macrophages. Methods Mol. Biol. *1784*, 263–275. https://doi.org/10.1007/978-1-4939-7837-3_24.
60. Fells, J.I., Lee, S.C., Fujiwara, Y., Norman, D.D., Lim, K.G., Tsukahara, R., Liu, J., Patil, R., Miller, D.D., Kirby, R.J., et al. (2013). Hits of a high-throughput screen identify the hydrophobic pocket of autotaxin/lysophospholipase D as an inhibitory surface. Mol. Pharmacol. *84*, 415–424. https://doi.org/10.1124/mol.113.087080.
61. Okudaira, M., Inoue, A., Shuto, A., Nakanaga, K., Kano, K., Makide, K., Saigusa, D., Tomioka, Y., and Aoki, J. (2014). Separation and quantification of 2-acyl-1-lysophospholipids and 1-acyl-2-lysophospholipids in biological samples by LC-MS/MS. J. Lipid Res. *55*, 2178–2192. https://doi.org/10.1194/jlr.D048439.

STAR★METHODS

KEY RESOURCES TABLE

REAGENT or RESOURCE	SOURCE	IDENTIFIER
Antibodies		
Brilliant Violet 510 anti-mouse CD45 (clone 30-F11)	BioLegend	Cat#103138; RRID: AB_2561392
Alexa Fluor 700 anti-mouse/human CD11b$^+$ (clone M1/70)	BioLegend	Cat#101222; RRID: AB_493705
Brilliant Violet 785 anti-mouse CD11c (clone N418)	BioLegend	Cat#117335; RRID: AB_11219204
Brilliant Violet 605 anti-mouse I-A/I-E (MHCII, clone M5/114.15.2)	BioLegend	Cat#107639; RRID: AB_2565894
PerCP-Cyanine5.5 anti-mouse F4/80 (clone T45-2342)	BD Bioscience	Cat#567202; RRID: AB_2916500
Allophycocyanin anti-mouse CD170 (SiglecF, clone S17007L)	BioLegend	Cat#155507; RRID: AB_2750236
Allophycocyanin/Cyanine7 anti-mouse Ly6C (clone HK1.4)	BioLegend	Cat#128025; RRID: AB_10640120
PE/Dazzle594 anti-mouse Ly6G (clone 1A8)	BioLegend	Cat#127647; RRID: AB_2566319
Brilliant Violet 421 anti-mouse CD206 (MMR, clone C068C2)	BioLegend	Cat#141717; RRID: AB_2562232
PE/Cyanine7 anti-mouse CD45 (clone 30-F11)	BioLegend	Cat#103113; RRID: AB_312978
Brilliant Violet 605 anti-mouse CD3 (clone 17A2)	BioLegend	Cat#100237; RRID: AB_2562039
Brilliant Violet 510 anti-mouse NK1.1 (clone PK136)	BioLegend	Cat#108738; RRID: AB_2562217
Allophycocyanin anti-mouse/rat/human CD27 (clone LG.3A10)	BioLegend	Cat#124211; RRID: AB_1236460
Alexa Fluor 488 anti-mouse/human CD11b$^+$ (clone M1/70)	BioLegend	Cat#101219; RRID: AB_493545
Allophycocyanin/Cyanine7 anti-mouse CD4 (clone GK1.5)	BioLegend	Cat#100413; RRID: AB_312698
PerCP-Cyanine5.5 anti-mouse CD8 (clone 53-6.7)	BioLegend	Cat#100733; RRID: AB_2075239
Brilliant Violet 421 anti-mouse CD107a (LAMP-1, clone 1D4B)	BioLegend	Cat#121617; RRID: AB_10896064
Alexa Fluor 700 anti-mouse FoxP3 (clone MF-14)	BioLegend	Cat#126421; RRID: AB_2750492
PE/Cyanine7 anti-mouse CD25 (clone 3C7)	BioLegend	Cat#101915; RRID: AB_2616761
PE/Dazzle594 anti-mouse CD279 (PD-1, clone 29F.1A12)	BioLegend	Cat#135227; RRID: AB_2566005
Brilliant Viollet 785 anti-human CD366 (Tim-3, clone F38-2E2)	BioLegend	Cat#345031; RRID: AB_2565832
Allophycocyanin anti-mouse Ly108 (CD352, clone 330-AJ)	BioLegend	Cat#134609; RRID: AB_2728154
Rat anti-4F1 ATX primary antibody	Gift from Dr. Junken Aoki, University of Tokyo; Available on MBL International	Cat# D323-3, RRID: AB_2819353

(*Continued on next page*)

Continued

REAGENT or RESOURCE	SOURCE	IDENTIFIER
Goat anti-rat HRP secondary antibody	Thermo Fisher Scientific	Cat#31470, RRID: AB_228356
Mouse anti-actin primary antibody	Sigma-Aldrich	Cat#MAB1501, RRID: AB_2223041
HPR-conjugated goat anti-mouse secondary antibody	Thermo Fisher Scientific	Cat#31430, RRID: AB_228307
Rabbit anti-CD11b primary antibody	Thermo Fisher Scientific	Cat#PA5-90724, RRID: AB_2806205
Goat anti-rat Alexa Fluor 488 secondary antibody	Thermo Fisher Scientific	Cat#A-11006, RRID: AB_2534074
Goat anti-rabbit Alexa Fluor 568 secondary antibody	Thermo Fisher Scientific	Cat#A-11011, RRID: AB_143157
Biological samples		
Human primary melanoma	Trimetis Life Sciences	Cat#111889 634A1
Human primary melanoma (neck)	Trimetis Life Sciences	Cat#111699 594A1
Human metastatic lung melanoma	Trimetis Life Sciences	Cat#111850 618A3
Human metastatic liver melanoma	Trimetis Life Sciences	Cat#109960 335B2
Chemicals, peptides, and recombinant proteins		
Polybrene	Sigma-Aldrich	Cat#TR-1003
Human recombinant ATX protein	Expressed and purified in house (UTHSC)	N/A
16:0-LPA	Avanti Polar Lipids	Cat#857123
17:0-LPA	Avanti Polar Lipids	Cat#857127
18:0-LPA	Avanti Polar Lipids	Cat#857128
18:1-LPA	Avanti Polar Lipids	Cat#857130
18:2-LPA	Avanti Polar Lipids	Cat#857138
20:4-LPA	Avanti Polar Lipids	Cat#857125
Critical commercial assays		
Platinum™ Direct PCR Universal Master Mix kit	Invitrogen	Cat#A44647500
HyStem® Hydrogel Kit	Advanced Biomatrix	Cat#GS311F
CD11b MicroBeads, human and mouse kit	Miltenyi Biotec	Cat#130-097-142
Super SignalTM West Atto Ultimate Sensitivity Substrate kit	Thermo Fisher Scientific	Cat#A38555
Hematoxylin & Eosin stain kit	Vector Laboratories	Cat#H-3502
Lung Dissociation Kit	Miltenyi Biotec	Cat#130-095-927
Zombie Green fixable viability kit	BioLegend	Cat#423112
Foxp3/Transcription Factor Staining Buffer Set	Invitrogen	Cat#00-5523-00
LEGENDPlex™ Mouse Inflammation Panel (13-plex)	BioLegend	Cat#740446
RNeasy RNA Extraction Micro Kit	Qiagen	Cat#74044
RevertAid Reverse Transcriptase Kit	Thermo Fisher Scientific	Cat#K1691
PowerUp Sybr Master Mix	Thermo Fisher Scientific	Cat#A25742
Deposited data		
Raw iwestern blots images	Mendeley Data	https://doi.org/10.17632/td7h8w9s32.1
T-distributed stochastic neighbor embedding (t-SNE) plots	Single Cell Portal[18,19]	https://singlecell.broadinstitute.org/single_cell
Experimental models: Cell lines		
Murine: B16-F10	ATCC	Cat# CRL-6475™; RRID: CVCL_0159
Murine: TdTomato B16-F10 (TdTB16-F10)	This paper	N/A

(*Continued on next page*)

Continued

REAGENT or RESOURCE	SOURCE	IDENTIFIER
Experimental models: Organisms/strains		
Mus musculus/B6.129P2-Lyz2$^{tm1(cre)Ifo}$/J	The Jackson Laboratory, JAX stock #018956	RRID:IMSR_JAX:018956
Mus musculus/ATX$^{fl/fl}$	Gift from Dr. Wouter H. Moolenaar, The Netherlands Cancer Institute, Amsterdam, NL[23]	N/A
Oligonucleotides		
Refer to Table S3		
Recombinant DNA		
EF1α-TdTomato lentiviruses	SignaGen Laboratories	Cat#SL100289
Software and algorithms		
FlowJo	FlowJo, version 10.10, BD Life SCiences	https://www.flowjo.com/; RRID:SCR_008520
Prism10	GraphPad version 10.1.0	https://www.graphpad.com/ RRID:SCR_002798

EXPERIMENTAL MODELS AND HUMAN MATERIALS

Human materials

Blocks of human primary or metastatic melanoma tumors were obtained from TriMetis Life Sciences (Germantown, TN, USA; Table S2 includes the list of cases shown in Figure 1).

In vivo mouse models

All animal procedures were approved by the University of Tennessee Health Science Center (UTHSC) Institutional Animal Care and Use Committee (IACUC) and were in accordance with the Guide for the Care and Use of Laboratory Animals. B6.129P2-Lyz2$^{tm1(cre)Ifo}$/J mice (LysMcre) were obtained from The Jackson Laboratory (RRID:IMSR_JAX:004781; Bar Harbor, ME). Enpp2 floxed mice (ATX$^{fl/fl}$ that possess loxP sites flanking exons 6 and 7 of the *Enpp2* gene) were a gift from Dr. Wouter H. Moolenaar (The Netherlands Cancer Institute, Amsterdam, NL). Where indicated, all mouse experiments were performed using either female or male mice (2 to 4 months old) maintained in individually ventilated cages under specific pathogen-free conditions. LysMcre mice were crossed with ATX$^{fl/fl}$ mice to generate mice of the following genotypes: LysMcre ATX$^{fl/fl}$ (abbreviated as LysM-KO) from which ATX is deleted in myeloid cells and littermate age-matched LysM-Cre, ATX^{WT} (abbreviated as LysM-WT) serving as WT controls. Genotyping was performed using the Platinum™ Direct PCR Universal Master Mix (Invitrogen; San Diego, CA, USA). Primers used are listed in Table S3.

Melanoma cell lines

Murine B16-F10 melanoma cells (ATCC Cat# CRL-6475™, RRID:CVCL_0159) were cultured in Minimum Essential Medium (MEM; ThermoFisher Scientific) supplemented with 5% heat-inactivated Fetal Bovine Serum (FBS; Cytiva; Marlborough, MA, USA), 2 mM of L-glutamine (Thermo-Fisher Scientific), 1% MEM-sodium pyruvate (Thermo-Fisher Scientific), 1% MEM-vitamins (Thermo-Fisher Scientific), and 1% MEM non-essential amino acids (NEAA; Thermo-Fisher Scientific). Cells were cultured in a humidified incubator at 37°C and 5% CO_2. All cell stocks were tested to be negative for mycoplasma contamination. For all *in vivo* experiments, a fresh aliquot of B16-F10 cell stock was thawed and cultured for at least two passages (~5 days) before being inoculated into mice.

To generate B16-F10 cells that expressed a tandem dimer (Td) of the red fluorescent protein Tomato (TdTB16-F10), 6x10^4 B16-F10 cells were plated per well of a 12-well plate and transduced with EF1α-TdTomato lentiviruses (Cat # SL100289, SignaGen Laboratories; Frederick, MD, USA) in the presence of 6 μg/mL polybrene (Sigma-Aldrich, Saint-Louis, MO, USA). The optimal multiplicity of infection (MOI) was determined according to the manufacturer's protocol and an MOI of 40 was selected for transduction of B16-F10 cells. After transduction, cells were cultured for an additional four days before sorting for TdTomato-positive B16-F10 cells using a FACSAria Cell Sorter (BD Biosciences; Franklin Lakes, NJ, USA). Sorted cells were further validated for TdTomato expression with a Nikon Eclipse Ti-U inverted fluorescence microscope (Nikon Instruments Inc., Melville, NY, USA).

METHOD DETAILS

Sample collection

Blood was collected in EDTA-coated tubes (Sarstedt; Nümbrecht, Germany), centrifuged and plasma was rapidly isolated and stored at -80°C. Metastatic nodules on the lung surface were counted either visually or microscopically using a Nikon TiU inverted fluorescence microscope (Nikon Instruments Inc.; Melville, NY, USA). Lungs were inflated and stored in either 10% buffered formaldehyde (Thermo-Fisher

Scientific; Waltham, MA, USA) for immunostaining procedures or with MACS® tissue storage solution (Miltenyi Biotec; Bergisch Gladbach, Germany) for flow cytometry analyses.

Spontaneous and experimental metastasis models

In the SMM, mice were shaved to remove the fur surrounding the left flank 3 days prior to subcutaneous tumor inoculation. On the day of inoculation, $2.5x10^5$ TdTB16-F10 cells were suspended in a 1:1 ratio of culture media and Extragel from a HyStem® Kit (Advanced BioMatrix; Carlsbad, CA, USA), according to the manufacturer's instructions. 100 µL of cell suspension was inoculated subcutaneously into the left flank of each mouse. The primary tumor was measured with a caliper and weighed. In the EMM, 100 µl of culture medium containing $1.5x10^5$ TdTB16-F10 cells were inoculated intravenously via the tail vein. For quantification of TdTB16-F10 cells at D1, D3, and D14, whole lungs were excised and each lobe was carefully separated and imaged using the Nikon Eclipse Ti-U inverted fluorescence microscope.

Immunoblot analysis

Immunoblot analysis was performed as previously described.[35] Briefly, bone marrow cells were isolated from LysM-WT and LysM-KO mice. $CD11b^+$ myeloid cells were purified using the CD11b MicroBeads, human and mouse reagent (Miltenyi Biotech) according to the manufacturer's protocol. Protein extracted from $CD11b^+$ myeloid cells or from 2 µL of plasma was separated on a 7.5% BioRad TGX Stain-free gel system and activated under UV for 1 min before being transferred to nitrocellulose membranes. After blocking with TRIS-buffered saline 0.05% (v/v) Tween 20 (TBS-T) containing 5% (w/v) non-fat milk, the membranes were incubated with rat anti-4F1 ATX primary antibodies (1:1,000 dilution; gift from Dr. Junken Aoki, University of Tokyo, available on MBL International Cat# D323-3, RRID:AB_2819353), rinsed, and incubated with secondary goat anti-rat HRP antibodies (1:2,000 dilution; Thermo Fisher Scientific Cat# 31470, RRID:AB_228356). ATX protein was visualized using a Super Signal™ West Atto Ultimate Sensitivity Substrate kit (Thermo Fisher Scientific) for enhanced chemiluminescent detection. To determine equal loading of samples, membranes were stripped using Restore™ Western Blot Stripping Buffer (Thermo Fisher Scientific) and re-probed with mouse anti-actin primary antibodies (1:600,000 dilution; Sigma-Aldrich Cat# MAB1501, RRID:AB_2223041) and HPR-conjugated goat anti-mouse secondary antibodies (1:5,000 dilution; Thermo Fisher Scientific Cat# 31430, RRID:AB_228307). For plasma and supernatant samples, equal loading of samples were determined by normalizing to total protein using the stain-free gel system.

Histology and immunostaining of human samples

For histology analysis, 5 µm-paraffinized sections of human tissues were stained using a Hematoxylin & Eosin stain kit (Vector Laboratories, Newark, CA, USA). Immunohistology was used to probe for the expression of ATX, and CD11b (myeloid cells), on sections of human primary or metastatic melanoma tumors. After deparaffinization and rehydration, antigen retrieval was performed for 20 min at sub-boiling temperature in 10 mM citrate buffer, pH 6.0. Immunofluorescence staining was performed using the following primary antibodies: rat anti-4F1 (ATX) at a 1:100 dilution, and rabbit anti-CD11b (Thermo Fisher Scientific Cat# PA5-90724, RRID:AB_2806205) at a 1:100 dilution. The following Alexa fluor-conjugated secondary antibodies were all used at 1:1,000 dilutions: goat anti-rat AF488 (Thermo Fisher Scientific Cat# A-11006 (also A11006), RRID:AB_2534074), and goat anti-rabbit AF568 (Thermo Fisher Scientific Cat# A-11011 (also A11011), RRID:AB_143157). Sections were analyzed using a Zeiss 750 confocal microscope (Zeiss, Oberkochen, Germany).

T-SNE plots

t-SNE plots in Figures 1A and 1B were generated using the online Broad Institute Single Cell Portal (https://singlecell.broadinstitute.org/single_cell). For Figure 1A, scRNA-seq data of 31 clinical melanoma cases were deposited into the online portal.[18] t-SNE clustering was performed for 4,857 non-malignant cells present in these cases. For Figure 1B, 16,291 individual immune cells from 48 tumor samples of melanoma patients treated with checkpoint inhibitors were profiled.[19] ENPP2 and ITGAM expressions were projected onto the t-SNE plots to identify the populations of non-malignant cells that express these genes.

Flow cytometry

Lungs were dissociated using the Lung Dissociation Kit (Miltenyi Biotec). $2x10^6$ lung cells or erythrocyte-lysed spleen cells were transferred to each well of a V-bottom 96-well plate and stained with Zombie Green fixable viability kit (BioLegend, San Diego, CA). After pre-incubation of the cells with TrustStain FcX™ (BioLegend) for 10 min, cell surfaces were stained in FACS buffer (BioLegend) on ice for 20 min, and fixed in PBS supplemented with 2% formaldehyde. For the lymphoid panel, cells were fixed using a FoxP3 fixation/permeabilization staining kit (Thermo Fisher Scientific) according to the manufacturer's protocol. Cells were analyzed with a Bio-Rad ZE5 flow cytometer and the data were analyzed using FlowJo version 10.10 Software (RRID:SCR_008520, BD Life Sciences, Franklin Lakes, NJ, USA). Table S4 indicates the antibodies, dilutions and RRID used for the flow cytometry experiments. The markers used to identify each immune cell population are listed in Table S1.

Measurement of ATX activity

ATX activity was measured using the AMPLEX Red Choline release assay in concentrated conditioned medium (CM) of $CD11b^+$ myeloid cells isolated from the bone marrow of LysM-WT and LysM-KO mice. CM was collected after 18 h of incubation in serum-free medium, consisting of RPMI-1640 (Thermo Fisher Scientific), supplemented with 2 mM glutaMAX™ (Gibco, Grand Island, NY, USA) and 10 mM HEPES (Thermo

Fisher Scientific), clarified by centrifugation, filtered through a 0.22 μm filter, and concentrated using an Amicon Ultra 30kDa Centrifugal Filter (Millipore, Billerica, MA, USA). 20 μL of concentrated CM was added to 40 μL of assay buffer consisting of 50 mM Tris, 150 mM NaCl, 5 mM $CaCl_2$, 30 μM fatty acid–free BSA (pH 7.4), 0.1 U/ml choline oxidase (Thermo Fisher Scientific), 1 U/ml horseradish peroxidase (Thermo Fisher Scientific), 10 μM Amplex Red (Thermo Fisher Scientific), and 100 μM LPC (Avanti Polar Lipids, Alabaster, AL, USA).[60] Total assay volume of 60 μL was added to each well of a 96-well half area plate and ATX activity was measured in triplicate using the FlexStation 3 Plate Reader (Molecular Devices, San Jose, CA, USA) at excitation and emission wavelengths of 560 and 590 nm, respectively.

LPA quantification

All lysophospholipids (16:0-LPA, 17:0-LPA, 18:0-LPA, 18:1-LPA, 18:2-LPA, and 20:4-LPA) were purchased from Avanti Polar Lipids, Inc. 50 μL of EDTA-collected plasma were mixed with nine volumes of methanol acidified with 1 mM of ammonium formate, sonicated for 3 min, vortexed, and centrifuged at 14,000x g at 4°C for 10 min. The supernatant was separated and LC-MS/MS analysis was performed as previously described.[61] Briefly, a 10 μL sample was injected into the QTRAP 4500 LC-MS/MS instrument (AB Sciex, Framingham, MA, USA) and LC separation was performed with a Capcell Pak acidic resistance column (Shiseido, Tokyo, Japan) with a gradient of elution of solvent A (5 mM ammonium formate in water) and solvent B (5 mM of ammonium formate in acetonitrile). Both solvents were adjusted to pH 4.0 using formic acid. The elution program was as follows: 55% of solvent B for 10 min, followed by 10 to 30 min of a linear gradient to 85% of solvent B that was applied and held for 7 min, and the mobile phase was reset to 55% of solvent B for 3 min.

Measurement of cytokines

The levels of thirteen cytokines (IL-23, IL-1α, IFN-γ, TNF-α, MCP-1, IL-12p70, IL-1β, IL-10, IL-6, IL-27, IL-17A, IFN-β and GM-CSF) were measured by flow cytometry using the LEGENDPlex™ Mouse Inflammation Panel (BioLegend, San Diego, CA, USA).

Real-time quantitative PCR (RT-qPCR)

Total RNA was extracted using RNeasy Micro Kit (Qiagen, Germantown, MD) and transcribed to cDNA using the RevertAid Reverse Transcriptase Kit (Thermo Fisher Scientific). RT-qPCR was performed using the PowerUp SYBR Mastermix on a QuanStudio 6 system (Thermo Fisher Scientific) according to the manufacturer's protocol. Primers used are listed in Table S3.

QUANTIFICATION AND STATISTICAL ANALYSIS

Data were analyzed using GraphPad Prism version 10.1.0 software (RRID:SCR_002798, San Diego, CA). The choice of statistical tests was based on normality and sample size. Where indicated, the data from several independent experiments were pooled. The Shapiro-Wilk test was used to determine normality. Samples that passed the normal distribution test were analyzed with the parametric unpaired t-test with a two-tailed p-value. Mann-Whitney test was used for samples that do not meet parametric distribution. When comparing two independent variables, statistical analysis was performed using two-way ANOVA. p-values <0.05 (denoted *), <0.01 (denoted **) <0.001 (denoted ***) and <0.0001 (denoted ****) were considered to be statistically significant.